



Structural Neural Connectivity Analysis in Zebrafish With Restricted Anterograde Transneuronal Viral Labeling and Quantitative Brain Mapping

Manxiu Ma^{1,2†}, Stanislav Kler^{1,2†} and Y. Albert Pan^{1,2,3,4*}

¹ Center for Neurobiology Research, Fralin Biomedical Research Institute at VTC, Virginia Tech, Roanoke, VA, United States,

² Department of Neuroscience and Regenerative Medicine, Medical College of Georgia, Augusta University, Augusta, GA, United States, ³ Department of Biomedical Sciences and Pathobiology, Virginia-Maryland College of Veterinary Medicine, Virginia Tech, Blacksburg, VA, United States, ⁴ Department of Psychiatry and Behavioral Medicine, Virginia Tech Carilion School of Medicine, Roanoke, VA, United States

OPEN ACCESS

Edited by:

Qian-Quan Sun,
University of Wyoming, United States

Reviewed by:

Wolfgang Driever,
University of Freiburg, Germany
Kara Geo Pratt,
University of Wyoming, United States
Masahiko Hibi,
Nagoya University, Japan

*Correspondence:

Y. Albert Pan
yapan@vtc.vt.edu

[†] These authors have contributed
equally to this work

Received: 09 September 2019

Accepted: 30 December 2019

Published: 23 January 2020

Citation:

Ma M, Kler S and Pan YA (2020)
Structural Neural Connectivity Analysis
in Zebrafish With Restricted
Anterograde Transneuronal Viral
Labeling and Quantitative Brain
Mapping. *Front. Neural Circuits* 13:85.
doi: 10.3389/fncir.2019.00085

The unique combination of small size, translucency, and powerful genetic tools makes larval zebrafish a uniquely useful vertebrate system to investigate normal and pathological brain structure and function. While functional connectivity can now be assessed by optical imaging (via fluorescent calcium or voltage reporters) at the whole-brain scale, it remains challenging to systematically determine structural connections and identify connectivity changes during development or disease. To address this, we developed Tracer with Restricted Anterograde Spread (TRAS), a novel vesicular stomatitis virus (VSV)-based neural circuit labeling approach. TRAS makes use of replication-incompetent VSV (VSV Δ G) and a helper virus (lentivirus) to enable anterograde transneuronal spread between efferent axons and their direct postsynaptic targets but restricts further spread to downstream areas. We integrated TRAS with the Z-Brain zebrafish 3D atlas for quantitative connectivity analysis and identified targets of the retinal and habenular efferent projections, in patterns consistent with previous reports. We compared retinofugal connectivity patterns between wild-type and *down syndrome cell adhesion molecule-like 1 (dscaml1)* mutant zebrafish and revealed differences in topographical distribution. These results demonstrate the utility of TRAS for quantitative structural connectivity analysis that would be valuable for detecting novel efferent targets and mapping connectivity changes underlying neurological or behavioral deficits.

Keywords: transsynaptic, zebrafish, VSV, brain mapping, viral tracing

INTRODUCTION

The function of the brain is closely linked to its structure, i.e., how its billions of constituent cells are wired and connected by trillions of synapses. Understanding how these connections are formed and maintained is key to gaining mechanistic insight toward brain function and identifying the causes and treatments for neuropsychiatric disorders (Belmonte et al., 2004; Lynall et al., 2010; Fornito et al., 2015). Techniques for mapping the structure and function of the brain have progressed

rapidly in past decades, from anatomical structural analysis to functional computation, and from human participants to animal models (Kasthuri et al., 2015; Glasser et al., 2016). However, the large number of neurons and vast spatial scale of neuronal structures (from meters to nanometers) of the mammalian brain makes mapping neuronal networks at the cellular level and correlating them with development and disease a daunting task (Swanson and Lichtman, 2016).

Zebrafish (*Danio rerio*), a small tropical fish, has emerged as an accessible model for studying behavior, neuronal networks, and cellular connectivity (Orger and de Polavieja, 2017). Zebrafish has analogous neuroanatomy and neurochemistry to mammals and can perform complex sensory, motor, and cognitive functions during larval stages (5–10 days post fertilization, dpf). Importantly, at this stage, there are only roughly 100,000 neurons in the brain, 80% of which can be imaged and physiologically recorded in live, behaving animals (Ahrens et al., 2013; Chen et al., 2018; Abdelfattah et al., 2019). As a result, zebrafish whole-brain functional imaging studies have been able to generate cellular resolution neuronal activity maps under different behavioral contexts and linking activity maps to pathological states associated with autism spectrum disorder, schizophrenia, and epilepsy (Sakai et al., 2018; Thyme et al., 2019). The ability to fully interpret patterns of functional connectivity and determine causality for disorders, however, is limited by the lack of detailed structural information on neuronal wiring in zebrafish, which still lags behind other commonly used model organisms like mice, *Drosophila*, and *C. elegans*. Efforts are ongoing to map the full complement of neuronal connections (i.e., connectome) with electron microscopy in the larval and adult zebrafish, but the time and labor-intensive nature of synapse-level reconstruction has thus far restricted investigations to connections within smaller brain regions (Wanner et al., 2016; Hildebrand et al., 2017; Vishwanathan et al., 2017; Svava et al., 2018).

To address this, we sought to develop a virus and light imaging-based structural mapping technique that would allow for quantitative brain-wide mapping of neuronal connectivity in larval zebrafish. Previously, we found that recombinant vesicular stomatitis virus (VSV) can function as an anterograde transsynaptic tracer in a wide range of organisms (Mundell et al., 2015). VSV is a negative-strand RNA virus in the *Rhabdoviridae* family, which also includes the rabies virus (RABV). In contrast to RABV, which spreads retrogradely (from dendrite to presynaptic afferent axons), VSV spreads anterogradely (from efferent axons to their postsynaptic targets) when enveloped by its endogenous glycoprotein (VSV-G) (Beier et al., 2011b; Mundell et al., 2015). VSV injection into the retina of mice, chicken, and larval zebrafish led to highly efficient labeling of the optic nerve and targets of the visual pathway, including both direct retinorecipient connections and third-order neurons in areas further downstream.

These findings open the door for utilizing VSV for zebrafish structural circuit mapping. Substantial limitations, however, still remain. First, the spread of VSV is unrestricted, making it difficult to disambiguate direct (monosynaptic) and indirect (polysynaptic) connections. Second, replication-competent VSV and VSV-G expression are cytotoxic and lead to rapid

deterioration of health in larval zebrafish (Hoffmann et al., 2010; Mundell et al., 2015). Finally, there is no established method for quantifying and annotating viral labeling in zebrafish, which is necessary to correlate anatomical tracing with functional imaging.

In this study, we developed a novel approach utilizing replication-incompetent VSV (VSV Δ G) to achieve restricted anterograde transneuronal spread in zebrafish. We also developed an imaging and processing pipeline to register 3D image stacks to the widely used and extensively annotated Z-Brain digital atlas (Randlett et al., 2015). This method, termed TRAS (Tracer with Restricted Anterograde Spread), allows for a quantitative description of efferent connectivity based on neurotransmitter types and specific locations. We applied TRAS to investigate the axon projection patterns of retinorecipient cells and identified potential connectivity changes in zebrafish carrying a mutation in *down syndrome cell adhesion molecule-like 1* (*dscaml1*), a causal gene for autism spectrum disorder and human cortical abnormalities (Fuerst et al., 2009; Iossifov et al., 2014; Karaca et al., 2015; Galicia et al., 2018; Ma et al., 2020).

MATERIALS AND METHODS

Zebrafish Husbandry

Zebrafish (all ages) were raised under a 14/10 light/dark cycle at 28.5°C. Embryos and larvae were raised in water containing 0.1% Methylene Blue hydrate (Sigma-Aldrich). With the exception of *nacre* mutants, embryos were transferred to E3 buffer containing 0.003% 1-phenyl-2-thiourea (PTU; Sigma-Aldrich) to prevent pigment formation at 24 h post-fertilization. Developmental stages are as described by Kimmel et al. (1995). Sex was not considered as a relevant variable for this study, as laboratory zebrafish remain sexually undifferentiated until 2 weeks of age, beyond the stages being used (0–9 dpf) (Maack and Segner, 2003; Wilson et al., 2014). All experimental procedures are performed in accordance with Institutional Animal Care and Use Committee guidelines at Augusta University and Virginia Tech.

Transgenic and Mutant Zebrafish Lines

The *dscaml1*^{vt1} mutant line was generated by TALEN-targeted mutagenesis, which resulted in a seven base pair deletion and subsequent early translational termination (Ma et al., 2020). The *Tg(elavl3:H2B-GCaMP6f)* line was generously provided by E. Aksay at Weill Cornell Medicine, with permission from M. Ahrens at HHMI Janelia Research Campus (Kawashima et al., 2016). The *vglut2a:GFP* line [*Tg(slc17a6b:EGFP)*] was generously provided by J. Fetcho at Cornell University with permission from S. Higashijima at the National Institute for Basic Biology (Bae et al., 2009).

Preparation of VSV Δ G

VSV was prepared using methods detailed by Beier et al. (2016). 293T cells (ATCC, #CRL-3216) were transfected at 80% confluency on 75 cm² flasks with 7 μ g of *pCI-VSVG* plasmid (Addgene, #1733) and incubated overnight at 37°C. Afterward, cells were infected with VSV Δ G-RFP (VSV Δ G for short) (Beier et al., 2011b) at a multiplicity of infection (m.o.i.) of 0.1.

Viral supernatants were collected for the subsequent 3 days at 24-h intervals and combined. Cell debris was precipitated by centrifugation at 1,000 g for 20 min. To concentrate VSV Δ G, viral supernatant was ultracentrifuged for 3 h at 80,000 g with an SW32Ti rotor, and the pellet was resuspended in 100 μ l of culture medium. Viral stocks were titered by serial dilution on 90% confluent 293T cells. The number of fluorescent foci was calculated at 2 days post infection (dpi) by identifying RFP-positive cells. Typical viral titer was higher than 1×10^9 focus forming units/ml (ffu/ml).

For *in vitro* trans-complementation of VSV Δ G with lentivirus, BHK-21 cells (ATCC, #CCL-10) were seeded into 96-well plates and incubated overnight to reach 20,000 cells per well. Cells were co-infected with VSV Δ G (m.o.i. = 0.005) and VSV-G pseudotyped lentivirus (m.o.i. = 0–10,000) (lentivirus-SIN-CMV-eGFP or lentivirus-SIN-Ubi-iCre-mCherry; GT3 Core Facility of the Salk Institute). The typical viral titer for lentivirus stock was 10^{11} – 10^{12} ffu/ml. At 2 h post-infection, cells were washed twice with PBS and incubated with fresh medium supplemented with 2% serum. At 2 dpi, the spread of VSV was visualized by fluorescent microscopy. The media in each well were collected and titered to evaluate viral yield.

Virus Injection

Viral injections were performed as previously described (Mundell et al., 2015; Beier et al., 2016). Briefly, glass capillaries (TW100F-4; World Precision Instruments) were pulled into injection needles with a pipette puller (P-97; Sutter Instruments). The tips of injection needles were trimmed to create a $\sim 10 \mu$ m opening. Virus injection solution was made by diluting VSV Δ G and lentivirus stock with tissue culture medium (DMEM; Fisher Scientific), with Fast Green dye (BP123-10; Fisher Scientific) as the injection marker. Two microliter of injection solution was loaded into the injection needle with a Microloader pipette tip (930001007; Eppendorf), and mounted into a microelectrode holder connected to a pneumatic PicoPump (PV820; World Precision Instruments). Injection volume was determined by calibrating the volume of the injected droplet on a stage micrometer (50-753-2911; Fisher Scientific). The hold pressure of the PicoPump was adjusted so that there was a slight outflow of virus solution when the needle tip was immersed in media.

For retina injection, 2.5 or 3 dpf larvae were anesthetized in Tricaine (0.013% w/v, AC118000500; Fisher Scientific) mounted laterally inside the center chamber of a glass-bottom dish (P50G-1.5-14-F; MatTek) with 1.5% low melting-point agarose (BP1360; Fisher Scientific). After the agarose has solidified, the dish is filled with Tricaine solution (0.013%) to maintain anesthesia. Under a stereo dissecting microscope (SMZ18; Nikon), the needle tip was moved with a micromanipulator (MN-151; Narishige) to approach the fish from the rear and penetrated the temporal retina, with the needle tip being in the neural retina. 0.25–0.5 nl of virus solution (concentrations as described in the Results section) were injected inside the retina. After injection, larvae were recovered from the agarose and returned to a 28°C incubator.

For TRAS labeling, we adjusted viral titer with the aim of achieving cellular labeling in areas innervated by the optic nerve and not in areas two synapses away (e.g., ipsilateral

midbrain, hindbrain, cerebellum, habenula, telencephalon). VSV Δ G injected without lentivirus at 10^6 – 10^9 ffu/ml resulted in robust retinal infection at the injection site. When lentivirus (2×10^9 – 10^{11} ffu/ml) was injected along with VSV Δ G (10^6 – 10^8), transneuronal spread was observed. For quantitative analysis of retinorecipient cells, we used VSV Δ G at 3×10^7 ffu/ml and lentivirus at 3×10^{10} ffu/ml. At these concentrations, we did not see any evidence for multisynaptic spread. It is worth noting that we did find sparse labeling of putative third-order neurons in one experiment that had extensive infection (potentially due to aliquot-specific variations in viral titer) with VSV Δ G at 3×10^7 ffu/ml and lentivirus at 3×10^{10} – 10^{11} (1–2 cells in 50% of injected fish, $n = 10$, **Supplementary Figure S1**). We only analyzed the experiments that had no third-order neuron labeling in this study.

For habenula injection, 3 dpf larvae were mounted with the dorsal side up. The agarose and skin above the left habenula were carefully removed with a sharpened tungsten needle (10130-05; Fine Science Tools). The injection needle tip was inserted into the left habenula and remained there for 5 s, allowing the slow outflow of virus solution (VSV Δ G at 3×10^8 ffu/ml, lentivirus at 1×10^{11} ffu/ml) to immerse the surrounding tissue. At 1 dpi, larvae with habenula-specific RFP expression were screened and later fixed at 3 dpi for immunohistochemistry and confocal imaging.

Immunohistochemistry

Whole-mount immunohistochemistry was performed as described by Randlett et al. (2015). Zebrafish larvae were fixed overnight with 4% PFA and 0.25% Triton X-100 (Fisher Scientific) in 1X PBS (diluted from 10%PFA; Polysciences), then washed with 1X PBS and 0.25% Triton X-100. H2B-GCaM6f was stained with FluoTag-X4 anti-GFP (N0304-At488; NanoTag); GABA was stained with Rabbit anti-GABA (A2052; Sigma-Aldrich); ERK1/2 was stained with mouse anti-ERK1/2 (4696S; Cell Signaling Technology). The sRIMS solution, which is D-Sorbitol (Sigma-Aldrich) dissolved in PBS with 0.1% Tween-20 (Fisher Scientific) and 0.01% Sodium Azide, was used for optical clearing (Yang et al., 2014). Samples are immersed for 15 min (or until sunken to the bottom of the Eppendorf tube) through a gradient series (8.75–70%) of D-Sorbitol.

Image Acquisition

Epifluorescence images of cultured cells were acquired under a Nikon Eclipse Ts2 inverted fluorescent microscope. Images of zebrafish were acquired using a Nikon A1 laser scanning confocal system with a CFI75 Apochromat LWD 25x water-immersion objective. For TRAS quantification, image stacks were acquired at a standard resolution of $0.49 \times 0.49 \times 2.0 \mu\text{m}^3$ per voxel. For efferent tract-tracing, a standard resolution stack and a high-resolution stack ($0.38 \times 0.38 \times 0.5 \mu\text{m}^3$ per voxel) were acquired for each fish.

Efferent Tract Tracing

Standard resolution image stacks were morphed to the Z-Brain *elavl3:H2B-RFP* template using CMTK (Randlett et al., 2015). High-resolution stacks were then morphed to its

corresponding low-resolution stacks to register to Z-Brain coordinates. Morphed high-resolution stacks were imported into the neuTube software for tracing, in accordance with the neuTube online manual (<https://www.neutracing.com/manual/>) (Feng et al., 2015). The SWC files were saved and imported into Fiji plugin “Simple Neurite Tracer” then saved as an overlay.

TRAS Quantitation With Z-Brain

Image stacks from 24 wild-type and 26 *dscaml1*^{-/-} larvae were morphed to the Z-Brain *elavl3:H2B-RFP* template using CMTK, using the GCaMP6f channel as reference (Randlett et al., 2015). For retinal ganglion cell arborization field (AF) fluorescent intensity analysis, the *ZBrainAnalysisOfMAPmaps.m* MATLAB script from Z-Brain was used to process each morphed stack individually (VSVΔG channel, no smoothing). From the output files, the total signal intensities from all Z-Brain annotated AFs (AF1-AF9 and the tectum neuropil) from each stack were then compiled and analyzed in the Prism statistical software (GraphPad).

For retinorecipient cell number and distribution analysis, the Fiji software’s ROI manager (Analyze > Tools > ROI manager; extra-large size dot) was used on the morphed VSVΔG channel to mark all VSVΔG+ cells. The marked positions (ROIs) were saved into a zip file and overlaid onto the GCaMP6f channel. The ROIs that were GCaMP6f-negative were removed so that the remaining ROIs represented TRAS-labeled neurons (neuronal ROIs). Next, the neuronal ROIs were overlaid onto the GABA channel to create two subsets: the GABA+ ROIs (inhibitory neurons) and GABA- ROIs (excitatory neurons, created by subtracting the neuronal ROI with the GABA+ ROIs). Lastly, these two ROIs were overlaid onto a Z-brain reference-sized (X:Y:Z = 1,121 × 496 × 276 μm³ at 0.8 × 0.8 × 2 μm³ per voxel) blank stack, with inhibitory neuron ROIs pseudo-colored magenta and excitatory neuron ROIs pseudo-colored green. Then, we created .tif files with the overlaid ROIs.

To quantitate the anatomical distribution of retinorecipient cells, we used a modified Z-Brain workflow. Instead of using the *MakeTheMAPmap.m* MATLAB script, we used a custom Fiji macro script to create the output image file, which were then processed using a modified *ZBrainAnalysisOfMAPmaps.m* MATLAB script that quantifies sum pixel intensity values for neuronal ROIs within each region mask. The output intensity values were converted to cell counts, based on an estimate of the pixel values generated from a single-cell ROI (~18,265). For heatmap display and cohort-wise comparison of individual regions, the intensity signals for each fish were normalized by the sum signal from “Diencephalon” and “Mesencephalon.” The numbers were then imported into MATLAB to make a scaled color map using the *imagesc* function.

Analysis of Topographical Distribution

To analyze the topographical distribution of wild-type and *dscaml1*^{-/-} retinorecipient cells (Figure 5), the ROI files from all fish within a cohort were combined into a single zip file and overlaid into a Z-Brain compatible blank stack, as described previously for single fish ROI image files. The x-y-z coordinates of each ROI dot were used in the *scatter3* function in MATLAB

to create 3-D scatter plots. The same coordinates were imported into GraphPad for analysis of distribution properties. The cumulative frequency statistics were done using the K-S test provided within the Prism software (GraphPad).

RESULTS

Trans-complementation of VSVΔG by VSV-G Coated Lentivirus

For both VSV and RABV, the envelope glycoprotein (G) gene is essential for binding, internalization, membrane fusion, and release of the viral genome into the host cell (Albertini et al., 2012; Kim et al., 2017). A recombinant virus with genomic deletion of the G gene (ΔG) can infect and replicate inside the cell but is unable to spread, unless the host cell complements the virus by providing G *in trans* (Wickersham et al., 2007; Beier et al., 2011b). Trans-complementation can, therefore, be utilized to restrict viral spread to direct synaptic partners. For instance, expressing the RABV glycoprotein (RABV-G) in neurons at the injection site (starter cells) allowed VSVΔG or RABVΔG to spread from the starter cells to their input neurons. Once inside the input neurons, the virus can no longer spread (Wickersham et al., 2007; Beier et al., 2013).

Given VSV’s ability to spread anterogradely across synapses, we asked whether trans-complementing VSVΔG virus with VSV glycoprotein (VSV-G) could enable restricted anterograde spread (Mundell et al., 2015). Our efforts to express VSV-G *in vivo* through transgenesis were unsuccessful, possibly due to the pathogenic effects of VSV-G when persistently expressed (Yee et al., 1994). As an alternative, we tested whether VSV-G protein could be transduced to cells directly. We took advantage of the fact that most commercially available lentiviruses are coated with VSV-G and examined whether concomitant VSVΔG/lentivirus infection could provide sufficient VSV-G to trans-complement VSVΔG *in vitro*. 293T cells were co-infected with VSV-G enveloped, RFP-expressing VSVΔG at low density (m.o.i. = 0.005) and lentivirus at a range of densities (m.o.i. = 0–1,000). At 2 days post-infection (dpi), we visualized the spread of VSVΔG by fluorescent microscopy and determined the yield of newly synthesized VSVΔG in the media. Indeed, lentivirus complemented VSVΔG in a dose-dependent manner, indicating that VSV-G on the envelope of lentivirus could be taken up by VSVΔG to form functional virions (Figures 1A–C).

Lentivirus-mediated trans-complementation was also effective *in vivo*, enabling transneuronal spread. By itself, VSVΔG injection into the eye (0.5 nl at 10⁸ ffu/ml) resulted in retina infection and RFP labeling of the optic nerve, but no cellular labeling in the brain (Figures 1D,E). This suggested that VSVΔG was not released from axon terminals to initiate a new cycle of infection in the brain. When low (5 × 10⁹ ffu) or high titer lentivirus (2 × 10¹⁰ ffu) was co-injected with VSVΔG (10⁸ ffu/ml), we observed cellular labeling in the brain in both conditions, with more spread in injections with high titer lentivirus (Figures 1F,G). This agrees with our *in vitro* results

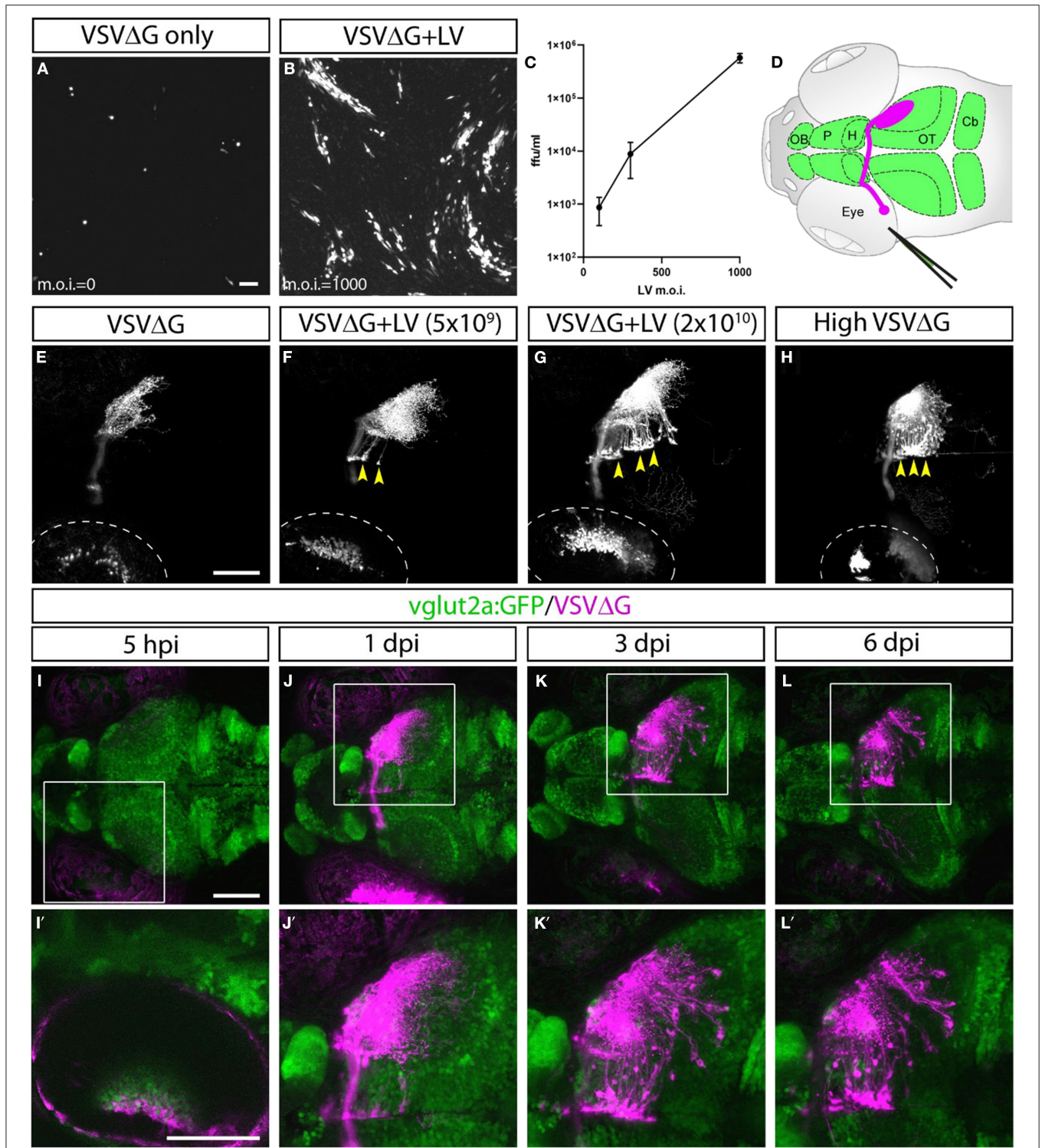


FIGURE 1 | Lentivirus enabled *in vitro* and *in vivo* trans-complementation of VSVΔG and transneuronal spread. **(A–C)** Lentivirus trans-complementation *in vitro*. **(A)** VSVΔG was able to infect 293T cells but was unable to spread to neighboring cells, as evident by sparse single-cell infections. **(B)** In conjunction with lentivirus, VSVΔG was able to both infect and spread, as evident by the presence of large infected plaques. **(C)** The extent of VSVΔG amplification (as measured by viral titer) is positively correlated with lentivirus titer, expressed in m.o.i. **(D)** Illustration of viral injection and labeling of the optic nerve. Virus was microinjected into the left eye, which infected the RGC and resulted in fluorescent labeling of the RGC axons (magenta). The layout of the larval CNS is labeled in green, with the olfactory bulb (OB), pallium (P), habenula (H), optic tectum (OT), and cerebellum (Cb) labeled. **(E–H)** *In vivo* trans-complementation of VSVΔG by lentivirus. In the absence of lentivirus, (Continued)

FIGURE 1 | VSVΔG infected RGCs and fluorescently labeled the optic nerve, but no spread in the CNS was observed (**E**). (**F,G**) When lentivirus and VSVΔG were coinjected, cellular labeling was observed in the CNS (yellow arrowheads), indicating transneuronal spread. (**H**) Similar patterns of spread was also seen at very high VSVΔG titer (2×10^9 vs. 10^9 ffu/ml for **E–G**), suggesting that VSVΔG was able to self-complement. (**I–L**) Time course of VSVΔG infection and spread with lentivirus trans-complementation, with RFP expression from VSVΔG (magenta) and GFP expression from the *vglut2a:GFP* transgene (green). Box regions are shown at higher magnifications below (**I'–L'**). Scale bars are 100 μm. Images in the same row are shown at the same scale.

and indicates that high titer lentivirus can trans-complement VSVΔG, allowing viral spread from axon terminals.

The ability of lentivirus to trans-complement was not dependent on what the lentivirus genome encodes. Two types of VSV-G coated lentivirus were tested (lentivirus-SIN-CMV-eGFP and lentivirus-SIN-Ubi-iCre-mCherry). Both were able to mediate trans-complementation, and neither were able to drive transgene expression (eGFP and iCre-mCherry, respectively) on their own in fish at 6 dpi. Lastly, we asked whether VSVΔG could self-complement at higher titer since VSVΔG itself was also enveloped in VSV-G. Indeed, high titer VSVΔG (2×10^9 ffu/ml) could spread from the retinal ganglion cell (RGC) to retinorecipient cells in the brain (**Figure 1H**). Together, these results show that VSV-G from different viral particles could be recycled to form infectious VSV particles. The use of lentivirus provides the additional flexibility to adjust VSVΔG and lentivirus titers to optimize for the extent of starter cell infection and transneuronal spread for sparse or dense labeling (e.g., **Figures 1E,G**).

Restricted Anterograde Spread of VSVΔG in the Zebrafish Visual Pathway

Since lentivirus was supplied at the injected site, only neurons at the injection site (starter cells) should be able to mediate spread. The spread from the starter cells should be limited to direct postsynaptic targets, i.e., anterograde monosynaptic spread. To test this, we examined whether the spatial and temporal patterns of VSVΔG spread were consistent with monosynaptic spread from RGCs to retinorecipient neurons in the brain.

VSVΔG and lentivirus were coinjected into the left temporal retina of anesthetized 3 dpf zebrafish larvae, followed by live confocal imaging at different time points ($n = 9$ animals). Initial RFP expression from VSVΔG was present in the injected (left) eye as early as 5-h post infection (hpi) (**Figures 1I–I'**). Cellular labeling in the contralateral (right) brain was observed at 1 dpi, and more cells were labeled at 3 dpi (**Figures 1J–K'**). At 6 dpi, there was no further spread to other brain regions, compared to 3 dpi (**Figures 1L–L'**). This pattern of labeling is distinct from non-G-deleted (i.e., replication competent) VSV, which rapidly progressed from axonal labeling to cell body labeling in downstream areas like the cerebellum and habenula at 3 dpi (Mundell et al., 2015). These results suggest that lentivirus trans-complementation primarily mediated anterograde monosynaptic spread. We call this new technique Tracer with Restricted Anterograde Spread, or TRAS (pronounced like *trace*).

Efferent Projections of Retinorecipient Cells Were Revealed by TRAS

Retinorecipient cells extend axons to different parts of the brain to mediate visually guided cognitive, sensory, motor, and

homeostatic functions. Previous studies have utilized transgenic reporter lines to characterize efferent projections of subsets of retinorecipient cells, but there has not been a method that could unbiasedly label retinorecipient cells in different brain regions and reveal their efferent projections (Zhang et al., 2017; Helmbrecht et al., 2018; Kramer et al., 2019).

With TRAS, we observed several prominent efferent tracts from retinorecipient neurons, innervating the telencephalon (6 of 9 animals), habenula (2 of 9), tegmentum (8 of 9), contralateral optic tectum (8 of 9), cerebellum (7 of 9), and along the ventral hindbrain (7 of 9) (**Figure 2**, image stack for **Figure 2A** is shown in **Supplementary Video 1**). The less frequently observed efferent projections (i.e., habenula) likely originate from a smaller retinorecipient cell population that was less frequently labeled by the stochastic spread of virus from RGC axon terminals. Overall, these projection patterns are reminiscent of the efferent projections of putative tectal/pretectal retinorecipient neurons identified by sparse transgenic labeling or single-cell photoconversion, further supporting the idea that TRAS primarily labels retinorecipient cells (Sato et al., 2007; Helmbrecht et al., 2018; Kramer et al., 2019). The projection into the telencephalon by retinorecipient neurons, to our best knowledge, has not been reported previously. These axon projections extend rostrally to enter the subpallium and then course dorsally to the caudal pallium. Some axons crossed near the anterior commissure. These pallium-projecting neurons may serve similar roles as the mammalian lateral geniculate neurons to relay sensory information to higher visual areas (Mueller, 2012). These results show that TRAS could be used to identify not only postsynaptic cells but also downstream areas innervated by these cells.

3D Mapping and Cell-Type Characterization

To quantify connectivity patterns, we registered TRAS-labeled image stacks to the Z-Brain zebrafish brain atlas (Randlett et al., 2015). Transgenic fish expressing neuronal-localized nuclear GCaMP6f (*elavl3:H2B-GCaMP6f*) were injected at 2.5 dpf, into the temporal region of the left eye (representing the frontal visual field). Under these conditions, viral infection in the retina is predominantly in the temporal quadrant of the eye (examples of starter cell infection in animals with non-pigmented retina are shown in **Supplementary Figure S2A**). Infected larvae were fixed at 3 dpi and stained with anti-GFP (to amplify the GCaMP6f signal) and anti-GABA. Stained samples were then cleared in sRIMS, a sorbitol-based mounting media that was crucial to resolving single cells and axon tracts in the ventral brain (Yang et al., 2014) (**Figures 3A,B**, **Supplementary Figures S2B,C**). By extracting the Z-Brain *elavl3:H2B-RFP* stack from ZBrainViewer as the reference, image stacks were morphed and aligned

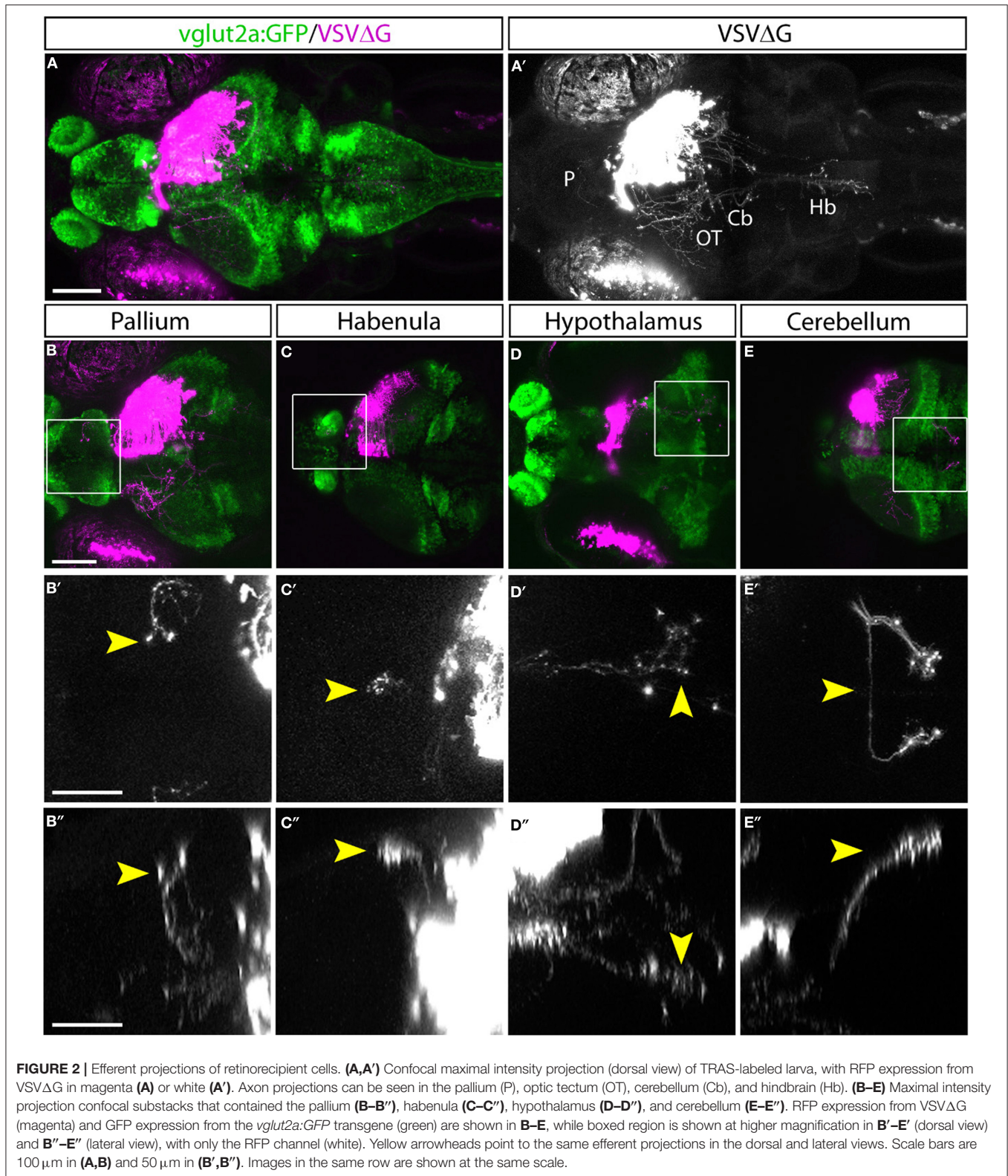
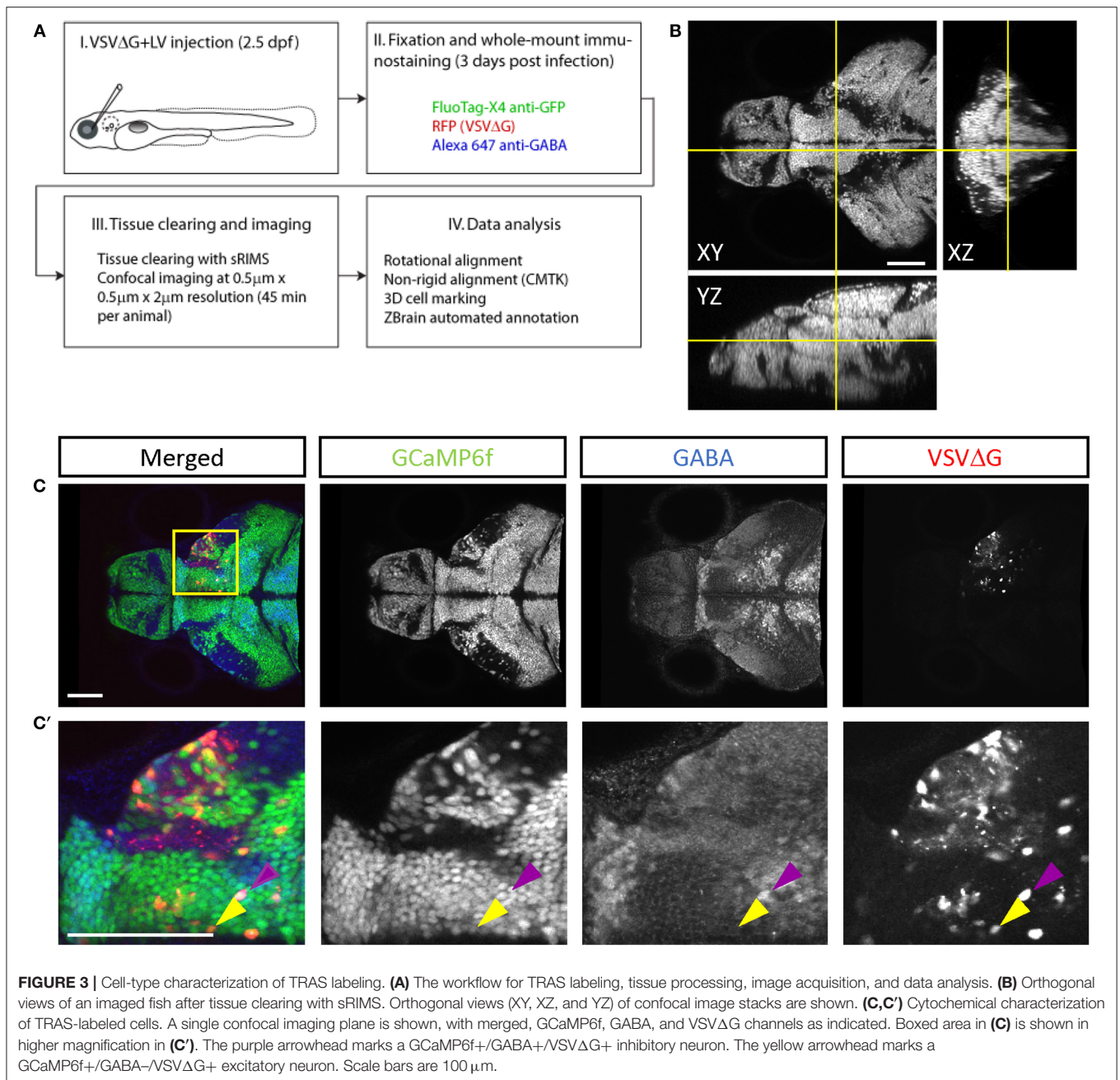


FIGURE 2 | Efferent projections of retinorecipient cells. **(A,A')** Confocal maximal intensity projection (dorsal view) of TRAS-labeled larva, with RFP expression from VSVΔG in magenta **(A)** or white **(A')**. Axon projections can be seen in the pallium (P), optic tectum (OT), cerebellum (Cb), and hindbrain (Hb). **(B–E)** Maximal intensity projection confocal substacks that contained the pallium **(B–B')**, habenula **(C–C')**, hypothalamus **(D–D')**, and cerebellum **(E–E')**. RFP expression from VSVΔG (magenta) and GFP expression from the *vglut2a:GFP* transgene (green) are shown in **B–E**, while boxed region is shown at higher magnification in **B'–E'** (dorsal view) and **B''–E''** (lateral view), with only the RFP channel (white). Yellow arrowheads point to the same efferent projections in the dorsal and lateral views. Scale bars are 100 μm in **(A,B)** and 50 μm in **(B',B'')**. Images in the same row are shown at the same scale.

with the Computational Morphometry Toolkit (CMTK) (Rohlfing and Maurer, 2003; Jefferis et al., 2007; Randlett et al., 2015).

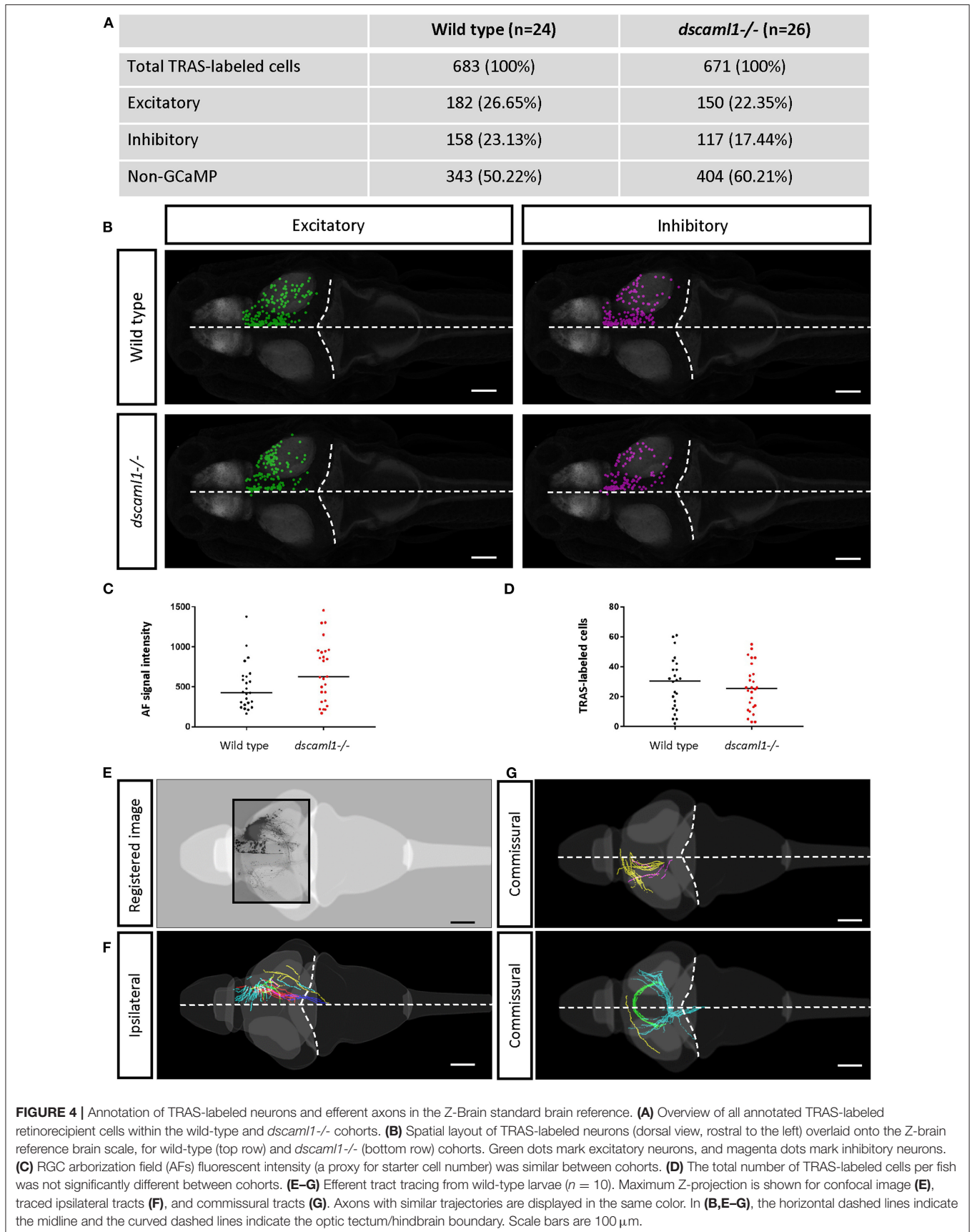
To distinguish different cell types, both transgenic and immunohistochemical markers were used. Nuclear GCaMP6f (expressed only in neurons) was used to distinguish between



neuronal (GCaMP6f+) and GCaMP6f non-expressing (GCaMP6f-, non-neuronal cells and GCaMP6f-negative neurons) cells (**Supplementary Figure S3**). Anti-GABA staining was used to distinguish between non-GABAergic and GABAergic (inhibitory) neurons (Cui et al., 2005) (**Figures 3C-C'**). Since glycinergic neurons are not present in the retinorecipient areas, non-GABAergic retinorecipient neurons are mostly excitatory, with potential inclusion of some GABAergic neurons without soma-localized GABA. After image morphing with CMTK, all TRAS labeled cells were converted into Z-Brain coordinates and categorized into three types: excitatory neurons (GCaMP6f+, GABA-) inhibitory neurons (GCaMP6f+, GABA+), and

GCaMP6f- cells. In total, 24 wild-type and 26 *dscaml1*^{-/-} fish (Ma et al., 2020) (see next section) were analyzed (**Figures 4A,B**, **Supplementary Video 2**). The overall ratio of excitatory vs. inhibitory cells was similar between wild-type and *dscaml1*^{-/-} cohorts ($p = 0.515$, Chi-square = 0.424). The annotated stack will be made available in the Z-Brain on-line viewer (<http://engertlab.fas.harvard.edu/Z-Brain/>) (Randlett et al., 2015).

The extent of starter cell (RGC) infection and subsequent spread was not significantly different between wild-type and *dscaml1*^{-/-} cohorts. To estimate the number of starter cells, we quantified the RFP fluorescence signal in the RGC arborization fields (AF1-10) (Burrill and Easter, 1994; Robles



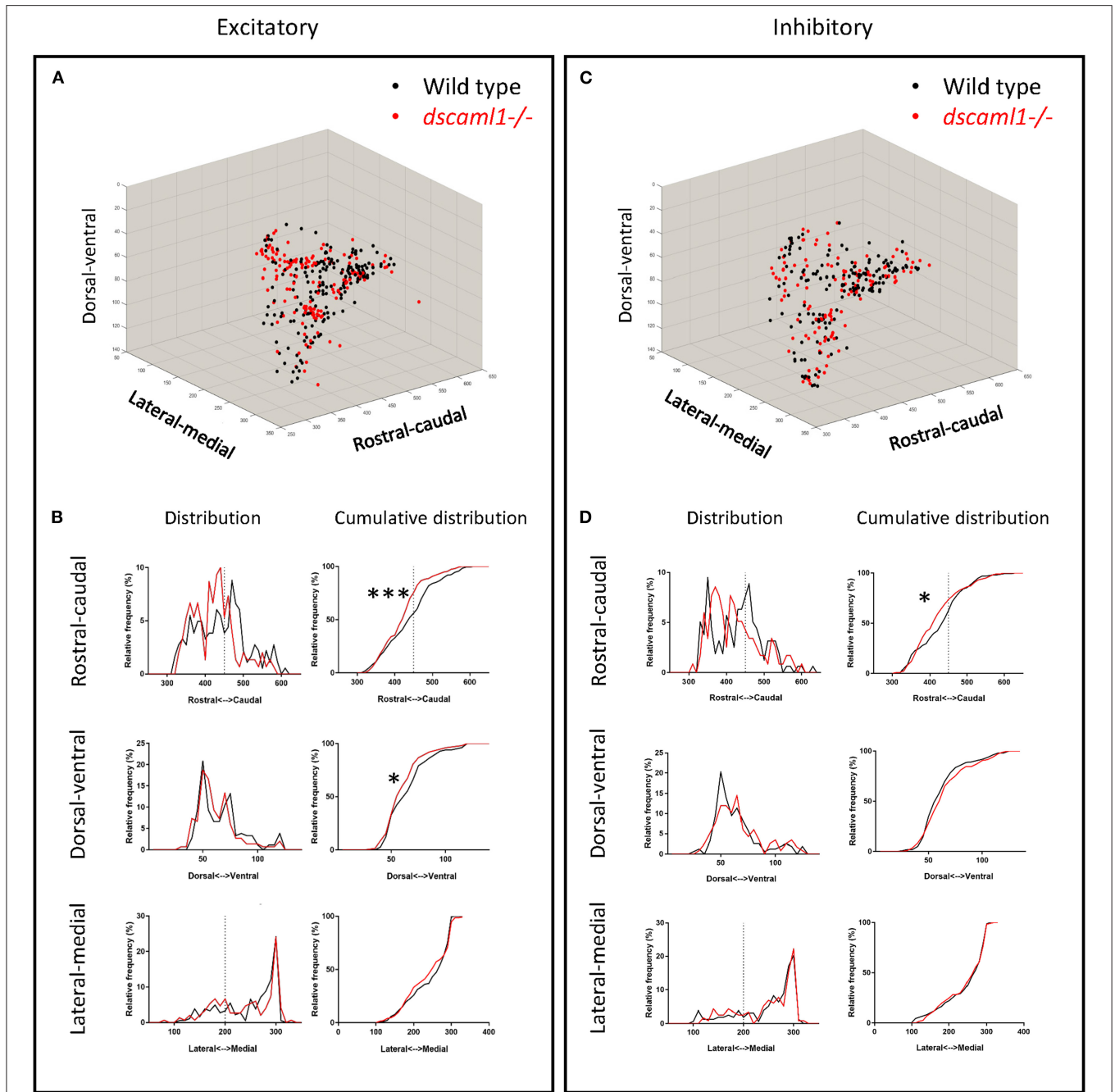


FIGURE 5 | Topographical organization of retinorecipient neurons in wild-type and *dscaml1*^{-/-} cohorts. Graphs show the topographical distribution of excitatory (A,B) and inhibitory neurons (C,D) in wild-type (black, *n* = 24) and *dscaml1*^{-/-} (red, *n* = 26) cohorts. Axes are relative distances (pixels) within the Z-Brain reference brain stack. (A,C) Three-dimensional distribution of excitatory (A) and inhibitory (C) neurons. (B,D) Frequency distributions of excitatory (B) and inhibitory (D) neurons in the rostral-caudal, dorsal-ventral, and lateral-medial axes. Dashed lines indicate the midpoints of the distributions. K-S test, **P* < 0.05; ****P* < 0.001.

et al., 2014), which are mostly derived from RGC axon terminals. There was no significant difference in arborization field fluorescence between cohorts, suggesting that the extent of starter cell infection was similar (Mann-Whitney *U*, *p* = 0.0932) (Figure 4C). The total number of TRAS-labeled retinorecipient cells were also not significantly different, suggesting similar

efficiencies in viral spreading between cohorts (Mann-Whitney *U*, *p* = 0.6335) (Figure 4D).

We verified that Z-Brain registered stacks could also be used as templates for tracing the efferent projections of retinorecipient cells (Figures 4E–G). We acquired high-resolution and low-resolution image stacks for the same fish

and used the high-resolution image stacks for tracing and low-resolution image stacks as the template to register to Z-Brain. We observed ipsilateral and commissural axon tracts, with morphologies that are similar to the tectal efferent tracts described in previous studies (Sato et al., 2007; Helmbrecht et al., 2018).

Comparative Analysis of Retinofugal Connectivity

In addition to normal patterns of retinofugal connectivity, TRAS and Z-Brain can be used to investigate retinofugal connectivity patterns in mutants with visual deficits. We focused on *Down Syndrome Cell Adhesion Molecule Like-1 (DSCAML1)*, a gene mutated in patients with autism spectrum disorder, cortical abnormalities, and developmental disorders (Iossifov et al., 2014; Karaca et al., 2015; Deciphering Developmental Disorders Study, 2017). In zebrafish, *dscaml1* is broadly expressed in visual areas and required for visual and visuomotor behaviors, suggesting an underlying visual circuit deficit (Ma et al., 2020). Therefore, we compared the retinofugal connectivity patterns between 5.5 dpf wild-type fish and their *dscaml1* mutant (*dscaml1*^{-/-}) siblings.

We asked whether the loss of *dscaml1* affected the topographical distribution of retinorecipient neurons (340 and 267 in wild type and *dscaml1*^{-/-}, respectively) (Figure 5). As the initial site of viral infection was in the temporal retina, these retinorecipient neurons likely respond to frontal visual stimuli. The overall distribution was similar between cohorts along the three cardinal axes, but the proportion of retinorecipient cells was significantly shifted in the rostral-caudal and lateral-medial axes. Along the rostral-caudal axis, both excitatory and inhibitory retinorecipient neurons from the *dscaml1*^{-/-} cohort were more rostrally distributed, compared to wild type ($p < 0.001$ and $p < 0.05$ for excitatory and inhibitory neurons, respectively, K-S test). Along the dorsal-ventral axis, the effect of *dscaml1* deficiency was milder. *dscaml1*^{-/-} retinorecipient cells were more dorsally distributed, compared to wild type, but only for excitatory neurons ($p < 0.05$, K-S test). There were no differences in lateral-medial distribution. These results suggest that loss of *dscaml1* may affect the topographic mapping of visual inputs, particularly along the rostral-caudal axes.

Next, we focused on the distribution of retinorecipient cells within specific annotated brain regions. We adapted the Z-Brain quantification tools to measure the sum pixel intensity derived from TRAS-labeled cells for each region (see methods). Among regions defined by anatomy (i.e., not defined by transgene expression), 16 were found to contain, on average, at least 1 retinorecipient cell per animal in the wild-type cohort (Figures 6A,C, Supplementary Figure S4). Two major brain divisions, the mesencephalon and diencephalon, encompassed all of the retinorecipient cells. Within these divisions, the retinorecipient cells are located within subregions corresponding to known to receive retinofugal input, including the preoptic area, hypothalamus, thalamus, eminentia thalami, pretectum, and optic tectum (tectum neuropil, tectum stratum periventriculare, and medial tectal band) (Burrill and Easter, 1994; Zhang et al., 2017; Helmbrecht et al., 2018; Kramer

et al., 2019). We saw no cellular labeling in the olfactory bulb (which innervates the retina), indicating that lentivirus complementation did not facilitate retrograde spread (Li and Dowling, 2000; Mundell et al., 2015). We also identified several retinorecipient areas that, to the best of our knowledge, had not previously been identified (torus semicircularis, tegmentum, posterior tuberculum). Some of these regions also receive retinorecipient efferent projections (tegmentum, poster tuberculum), as mentioned earlier.

In general, the same areas were innervated in both wild-type and *dscaml1*^{-/-} cohorts, except for two smaller areas that were not innervated in the *dscaml1*^{-/-} cohort (eminentia thalami and intermediate hypothalamus) (Figures 6A,C vs. Figures 6B,D). This result indicates that major retinorecipient areas are innervated by the optic nerve in the *dscaml1*^{-/-} animals.

TRAS Mapping of Habenular-Recipient Neurons

Finally, to test whether TRAS can be applied more generally to other CNS neuronal populations besides RGCs, we examined efferent targeting from the left habenula (Bianco and Wilson, 2009; Amo et al., 2010; Lee et al., 2010; Dreosti et al., 2014; Duboue et al., 2017; Zhang et al., 2017). The bilaterally asymmetrical habenula receives many different sensory cues and is involved in processing social cues, fear learning, and avoidance. The left habenula is known to project to the interpeduncular nucleus (IPN) and superior raphe, providing a suitable pathway to test TRAS mapping in the CNS (Bianco and Wilson, 2009; Amo et al., 2010). VSVΔG and lentivirus were injected into the left habenula of 3 dpf wild-type animals. At 3 dpi, animals for processed for anti-ERK1/2 immunostaining, confocal imaging, and image registration (see methods). Registered image stacks from five animals with selective left habenula labeling were combined (Figures 7A–C'). We observed consistent labeling of the habenular axon tract and the characteristic annular axon terminals in the IPN. Cell bodies near IPN axon terminals were manually marked (Figures 7D–E'). Consistent with previous findings, habenular target cells we labeled within the IPN and raphe nucleus (Amo et al., 2010). We did not observe efferent axons emanating from the habenular-recipient cells (Chou et al., 2016), which suggests that habenular-recipient projection neurons may be relatively rare at this stage. Overall, TRAS labeling in the retina and the habenula demonstrates the general applicability of TRAS for mapping the targets of efferent axons.

DISCUSSION

In this study, we developed TRAS, a new method for monosynaptic anterograde labeling in larval zebrafish. This method was applied to the retinofugal pathway and also validated in the habenula efferent pathway. We showed that TRAS could be combined with the Z-Brain image registration and quantitation pipeline to identify changes in retinofugal connectivity patterns caused by the loss of *dscaml1*. These results demonstrate the broad utility of TRAS for neural circuit studies in zebrafish.

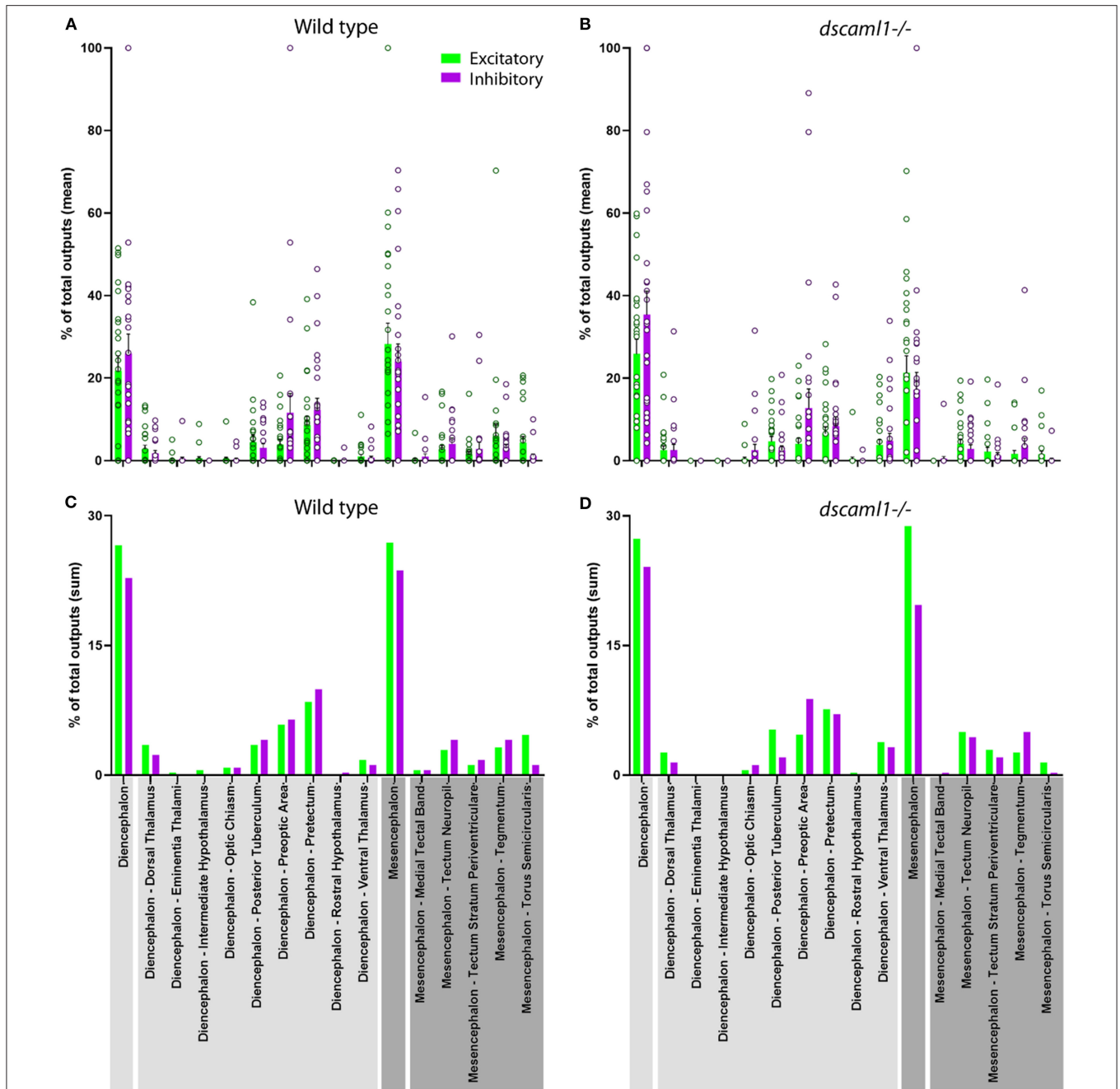


FIGURE 6 | Distribution of retinorecipient cells in annotated brain regions. The population means (A,B) and sums (C–D) of wild-type and *dscaml1*^{-/-} cohorts, divided by brain regions. Brain region names are noted in the bottom, with diencephalon and its subregions in light gray and mesencephalon and its subregions in dark gray. (A,B) For each wild-type and *dscaml1*^{-/-} animal, the percentage of total output was calculated by dividing the number of TRAS-labeled neurons within a region by the total number of TRAS-labeled neurons (both excitatory and inhibitory) in that animal. Individual data points, means, and standard errors are shown. (C,D) The percentage of total outputs was calculated by dividing the total number of TRAS-labeled neurons within a cohort by the total number of TRAS-labeled neurons (both excitatory and inhibitory) in that cohort.

Trans-complementation of VSVΔG by Lentivirus

The structure and function of VSV-G have been extensively studied in the context of viral entry, membrane fusion, toxicity, and subcellular transport (Dotti and Simons, 1990; Thomas

et al., 1993; Ang et al., 2004; Hoffmann et al., 2010; Albertini et al., 2012; Fossati et al., 2014; Kim et al., 2017). VSV-G also determines the infectivity of VSV-G coated viruses (VSV, RABV, lentivirus, retrovirus), which is crucial for their research and clinical applications (Wickersham et al., 2013; Amirache

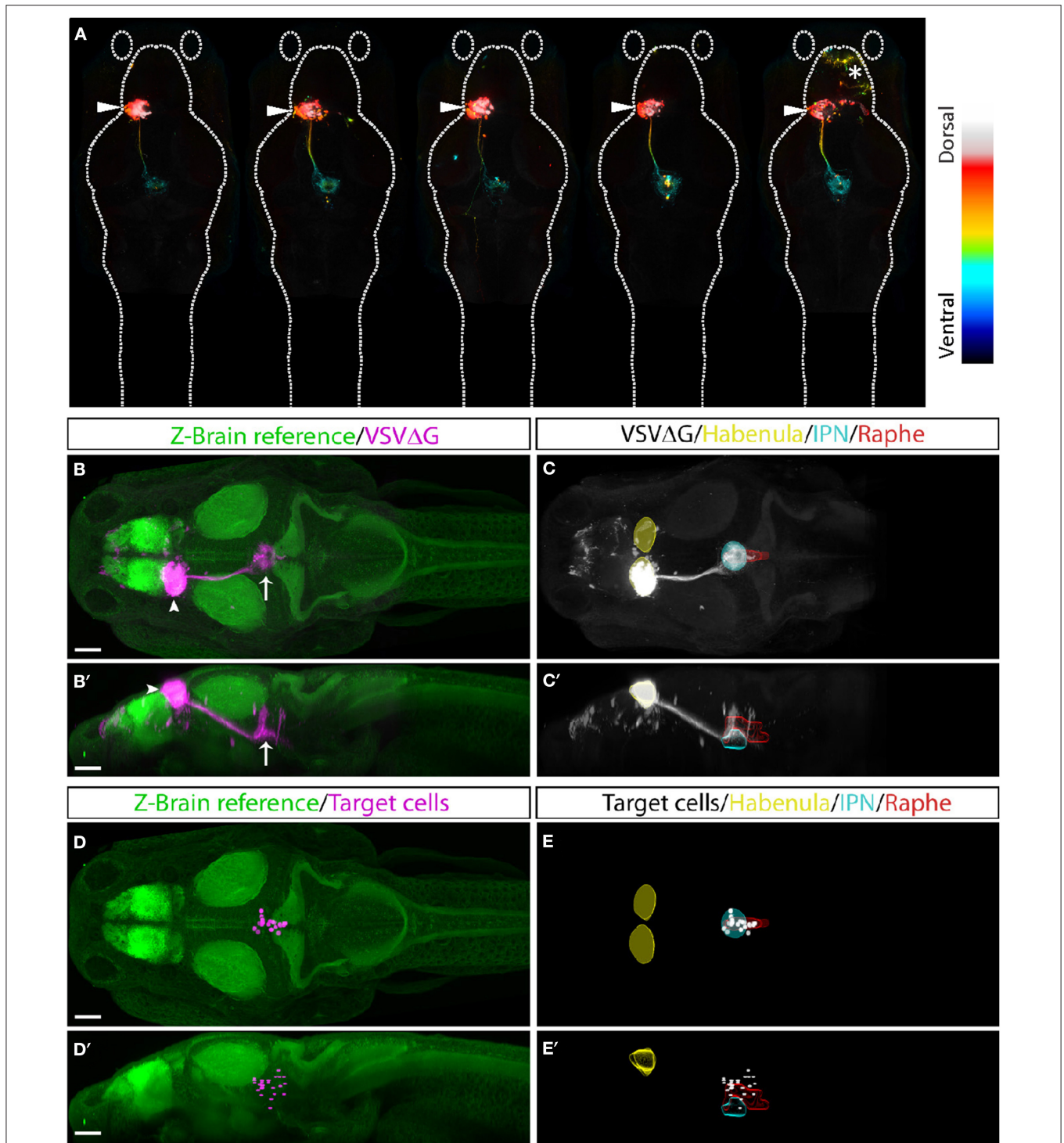


FIGURE 7 | TRAS labeling of habenular target cells. **(A)** Five fish with TRAS tracing from the left habenula (arrowhead), viewed dorsally. The z-dimension is color-coded, as indicated in the lookup table on the right. In one fish (far right), we observed infection in the telencephalon (asterisk). Given the absence of habenula to telencephalon efferents, these cells were likely infected by virus diffusion after injection. **(B–C’)** Combined maximal projection of registered image stacks from the animals shown in **(A)**. The left habenula (arrowhead) projects into the IPN (arrow). RFP expression from VSVΔG infection is shown in magenta **(B,B’)** or white **(C,C’)**. For anatomical reference, images are overlaid on top of the Z-Brain ERK1/2 reference stack (green, **B,B’**), or region outlines for the habenula (yellow), IPN (cyan), and raphe nucleus (red) **(C,C’)**. Dorsal **(B,C)** and lateral **(B’,C’)** views are shown. **(D–E’)** Manually marked habenular target cells (magenta in **D,D’**, white in **E,E’**) are overlaid on top of anatomical references, as described for **(A,B)**. Dorsal **(D,E)** and lateral **(D’,E’)** views are shown. Scale bars are 100 μm. All images are shown at the same scale.

et al., 2014; Mundell et al., 2015; Kobayashi et al., 2016). Our findings revealed a new aspect of VSV-G function, where VSV-G protein from a different viral species can be recycled to generate infectious VSV.

The spread of VSV Δ G from the retina to CNS neurons indicates that VSV-G on the lentivirus surface remained functional after lentivirus infection, and a portion of it was transported anterogradely from the cell body to the axon terminal. At the axon terminal, lentivirus-derived VSV-G was able to re-encapsulate the VSV nucleocapsid and mediate subsequent infection. Although it is possible to achieve transneuronal labeling with high titer of VSV Δ G, TRAS's two-virus system provides the flexibility of adjusting the titer of VSV Δ G based on the demand of the experiment (e.g., sparse vs. dense labeling), while maintaining robust transneuronal spread.

Additionally, the strategy of using lentivirus as a tool for glycoprotein complementation could potentially be applied more broadly. For example, current strategies for RABV monosynaptic tracing utilizes AAV to express RABV glycoprotein, which usually takes several weeks for sufficient glycoprotein expression (Miyamichi et al., 2011). It will be interesting to test whether rabies glycoprotein-coated lentivirus could be a more rapid method to provide glycoprotein for retrograde tracing.

Applying TRAS for Zebrafish Neural Connectivity Analysis

Advances in viral engineering have led to new neural circuit tracing strategies utilizing replication-incompetent viruses (e.g., RABV, AAV, HSV) that are safer to use, less toxic to host cells, and have restricted (mostly monosynaptic) spread (Wickersham et al., 2007; Zingg et al., 2017; Chatterjee et al., 2018; Beier, 2019). Unfortunately, many of the transsynaptic viruses used in mammalian systems either do not infect zebrafish (e.g., AAV) or have low efficiency for transsynaptic spread (e.g., RABV) (Zhu et al., 2009; Dohaku et al., 2019). VSV, in contrast, can infect larval zebrafish and spreads robustly both anterogradely and retrogradely. However, replication-competent VSV has high cytotoxicity and can spread across multiple synapses, making it difficult to distinguish between direct vs. indirect connections (Mundell et al., 2015).

To address these limitations and provide a tool for neural circuit mapping for larval zebrafish, we developed TRAS. TRAS utilizes recombinant VSV with genomic deletion of the glycoprotein gene (VSV Δ G). VSV Δ G can infect cells at the injection site but cannot spread. Although wild-type VSV does not cause serious illness to humans, the use of VSV Δ G further reduces the risk of exposure (Spickler, 2016). The lack of VSV-G expression from the viral genome also helps reduce toxicity to the host cell, as long-term VSV-G expression is known to be cytotoxic (Yee et al., 1994). To complement VSV Δ G, we directly provided VSV-G protein, utilizing lentivirus as the transducing reagent. Compared to transgenic or virus-induced expression, this approach is rapid and transient, therefore minimizing the cellular exposure to VSV-G. Both VSV Δ G and VSV-G coated lentivirus are available from a commercial source, making TRAS an easy method to adopt in a typical neuroscience laboratory.

To expand the utility of TRAS, we developed procedures to register brain images to the Z-Brain anatomical template (Randlett et al., 2015). The combination of neural circuit tracing within a standard 3D-brain atlas is the current state of the art approach for understanding neural network connections, both in zebrafish and mammalian models (Watabe-Uchida et al., 2012; Oh et al., 2014; Helmbrecht et al., 2018; Kramer et al., 2019; Kunst et al., 2019). This approach provides a more objective way to map cells and pathways onto specific brain regions across different experimental animals and promotes cross-referencing between research findings.

We demonstrated that TRAS and Z-Brain could be used for neural circuit mapping in efferent pathways originating from the retina and the left habenula. These are two of the better-studied pathways in larval zebrafish, which allowed us to assess the specificity of TRAS for anterograde labeling of direct postsynaptic targets. By applying TRAS to the habenula, we showed that TRAS could be used to map connections between regions within the central nervous system. It is interesting that we did not observe any efferent axons emanating from the habenular-recipient cells, given the known IPN output pathways described in the adult zebrafish (Chou et al., 2016). Further studies are needed to determine whether any habenular-recipient cells are projection neurons. Overall, TRAS identified all of the target regions described in previous studies, which gives confidence to the future application of TRAS to map unknown neural connections in zebrafish. Furthermore, given that VSV is also an anterograde tracer in mice and chicken, it will be interesting to test whether TRAS can be applied to these experimental systems for neural circuit mapping (Mundell et al., 2015).

Limitations and the Future Development of TRAS

While TRAS offers many advantages as a neural circuit mapping tool, it has similar limitations as other viral tracing techniques (Beier, 2019). In each injected animal, only a subset of the targeted starter cell population is infected, and only a subset of all connections from those starter cells are labeled by trans-neuronal spread. Therefore, the absence of TRAS labeling in a particular region in one animal does not equate an absence of connection in that animal. At the population level, patterns of spread may be affected by synaptic activity, physical distance, the age of the animal, selective biases of viral infection, and viral titer (Callaway and Luo, 2015). Here, we will discuss the limitations specific to TRAS and areas for further technological development.

Specificity of Initial Infection

Since VSV-G binds to a receptor that is widely expressed (LDL receptor) (Finkelshtein et al., 2013), VSV-G coated viruses can infect most cell types. Therefore, the specificity of TRAS depends on precise injection into the brain region of interest. For brain regions smaller than the habenula, a compound microscope with DIC optics would be necessary. To restrict infection to a particular cell type, it may be possible to make use of ASLV-A pseudotyped VSV Δ G that can selectively target neurons expressing an exogenous receptor, TVA (Beier et al., 2011b;

Dohaku et al., 2019). However, potential interactions between virions with different envelope glycoproteins may interfere with the specificity of VSV Δ G infection (Beier et al., 2011a).

Labeling of Direct vs. Indirect Synaptic Targets

Our analysis of retinorecipient cells indicates that TRAS spread anterogradely from the afferent axons to their direct targets. This is based on the fact that lentivirus is only present near the starter cells and that third-order neurons in downstream areas were rarely labeled. The pattern of TRAS labeling is notably more restricted compared to polysynaptic VSV, which labels third-order neurons within 3 days after initial infection (Mundell et al., 2015). However, we cannot rule out that some of the TRAS-labeled cells in primary retinorecipient areas may be indirectly connected to RGCs. Multiple approaches (e.g., electron microscopy, electrophysiology) will be needed to confirm findings from viral tracing.

Physiological Effects of Infection

While the lack of genomic VSV-G expression from VSV Δ G reduces toxicity, other genes expressed from the viral genome can still change the metabolism of the host cell. For instance, the VSV M protein is capable of altering host cell transcription and translation (Ahmed and Lyles, 1998; Connor and Lyles, 2005). Chronic VSV Δ G infection would likely affect the survival of infected neurons and impair its neurophysiological functions. Several approaches for reducing the toxicity of RABV have been reported recently to reduce the function or expression of viral proteins, such as destabilizing the RABV nucleoprotein or deleting the RABV L gene (Ciabatti et al., 2017; Chatterjee et al., 2018). Similar manipulations may also reduce the toxicity of VSV.

Cell-Type Characterization

We have used the *elavl3:H2B-GCaMP6f* transgene and GABA immunoreactivity as markers for post-mitotic neurons and inhibitory neurons, respectively. These markers are widely used in the zebrafish field (Mueller et al., 2006; Mueller and Wullmann, 2015), but it is likely that not all neurons express *elavl3*, and not all GABAergic neurons have GABA immunoreactivity in the soma. Further characterization of the *elavl3* and GABA-immunoreactive populations using alternative excitatory and inhibitory neuron markers (e.g., *vglut2*, *gad1b*) is needed to provide clarity on this issue (Satou et al., 2013).

Optimization of Viral Titer

The efficiency of TRAS depends on the titer of VSV Δ G and lentivirus as well as other factors specific to each experiment, including the condition and duration of virus storage, the tropism of virus to specific cell types, and the age/genetic background of the host. The viral titers for each type of application will need to be adjusted so that VSV Δ G by itself only labels the starter cells, and the addition of lentivirus enables robust monosynaptic spread (Figures 1E–G) (see methods). Low viral titer may result in the absence of labeling in more sparsely connected areas, whereas high viral titer increases the chance of VSV Δ G self-complementation at the axon terminal and multisynaptic spread.

Labeling of Retinorecipient Cells

With TRAS labeling, retinorecipient cells were strongly fluorescent, allowing us to observe and trace the retinorecipient cell efferent tracts. However, the dendritic morphologies of the retinorecipient cells were harder to discern, as the RGC afferents in the vicinity are labeled by the same fluorophore. This also made it difficult to trace the retinorecipient efferent axons back to their cellular origins. For mapping studies where the local projections or morphologies of the recipient cells are important, it will be beneficial to express a distinct fluorophore in the starter cells (e.g., from a transgene).

Mapping With Z-Brain

Z-Brain analysis depends on morphing and registration of image stacks to a reference template, followed by manual identification of labeled neurons. This approach is suitable to test the effects of single genes or pathological states, but likely too laborious as a screening tool to identify candidate genes or screen drugs. Selective fluorescent labeling of neuronal cell bodies (without labeling neurites) and automation of cell detection would be a crucial next step to improve the utility of TRAS.

Connectivity Patterns Associated With *dscaml1* Deficiency

The ability to quantitate efferent connections prompted us to investigate whether TRAS can be used to identify connectivity deficits caused by *dscaml1* deficiency. As mentioned previously, human DSCAML1 mutations are believed to be causative for neurodevelopmental disorders. Additionally, our recent work has found that loss of *dscaml1* significantly impaired visuomotor function associated with light perception and eye movements, suggesting a possible underlying deficit along the visual pathway (Ma et al., 2020).

Using TRAS and Z-Brain quantification, we found that *dscaml1* deficiency might have a role in refining the retinofugal topography and cell-type specificity. On a broader scale, we saw similar patterns of topographic and region-specific projections between wild-type and *dscaml1*^{-/-} cohorts (Figures 5, 6). This indicated that RGC axonal targeting was mostly intact in the *dscaml1* mutants. Interestingly, there was a significant rostral shift in the position in both excitatory and inhibitory retinorecipient cells. Given that RGC axon terminals and retinorecipient cells are both topographically organized, this shift in positioning may result in diminished spatial perception (Stuermer, 1988; Muto et al., 2013; Robles et al., 2014). Further physiological studies will be needed to formally test whether *dscaml1* affects spatial perception in the visual pathway.

CONCLUSIONS

Here, we present the development of TRAS, a new technique that is suitable for mapping neural connectivity in zebrafish. TRAS makes use of a novel lentivirus trans-complementation approach to enable restricted anterograde transneuronal spread by recombinant VSV. We have validated this method in two efferent pathways and identified potential connectivity pattern changes caused by a genetic deficiency in *dscaml1*, a neuronal cell adhesion molecule associated with human neurodevelopmental

disorders. The ability of TRAS to map structural connectivity would enable the discovery of new neural connections and complement existing brain mapping efforts.

DATA AVAILABILITY STATEMENT

The image stacks and other data supporting the findings of this study are available from the corresponding author upon reasonable request. Custom Fiji and MATLAB scripts used of this study are available from the corresponding author upon reasonable request.

ETHICS STATEMENT

The animal study was reviewed and approved by the Institutional Animal Care and Use Committees at Augusta University and Virginia Tech.

AUTHOR CONTRIBUTIONS

MM, SK, and YP conceived the study, performed the experiments, and analyzed the data. SK prepared and characterized recombinant viruses. MM and YP wrote the manuscript, with contributions from SK.

FUNDING

This work was supported by funding from the National Eye Institute of the National Institutes of Health (R01 EY024844 to YP), Center for Innovative Technology (ER14S-001-LS to YP), Augusta University, and Virginia Tech.

ACKNOWLEDGMENTS

We thank the animal care staff at Augusta University and Virginia Tech for animal husbandry, Owen Randlett for help with Z-Brain analysis, Didem Gotz Ayturk, Xiang Ma, and Constance Cepko for reagents and technical expertise for virus

preparation, and members of the Pan lab for helpful suggestions on the manuscript.

SUPPLEMENTARY MATERIAL

The Supplementary Material for this article can be found online at: <https://www.frontiersin.org/articles/10.3389/fncir.2019.00085/full#supplementary-material>

Supplementary Figure S1 | Examples of third-order neuron labeling. Red arrowheads indicate third-order neurons labeled in the hindbrain by TRAS. Yellow dash line marks the border of mesencephalon and cerebellum. Scale bar: 50 μ m.

Supplementary Figure S2 | Retina injection and tissue clearing. **(A)** Examples of RFP expression in the retina of unpigmented (PTU-treated) animals 3 days after virus injection into the temporal retina. Images are lateral views, with rostral side to the left and dorsal side to the top. Yellow dashed lines outline the eye (outer oval) and lens (inner oval). **(B,C)** Tissue clearing with sRIMS solution. Whole-mount ERK1/2 immunolabeling without **(B)** or with sRIMS clearing **(C)**. Orthogonal views (XY, XZ, and YZ) of confocal image stacks are shown, centered just below the cerebellum (intersect of yellow lines). Ventral structures are not visible without sRIMS clearing. Scale bars are 100 μ m.

Supplementary Figure S3 | TRAS labeling of GCaMP6f positive and negative cells. A single confocal imaging plane is shown, with merged, GCaMP6f, GABA, and VSV Δ G channels as indicated. Boxed area in **(A)** is shown in higher magnification in **(A')**. The purple arrowheads mark two GCaMP6f+/GABA+/VSV Δ G+ inhibitory neurons. The orange arrowhead marks a GCaMP6f-/GABA-/VSV Δ G+ cell. Scale bars are 100 μ m.

Supplementary Figure S4 | Signals detected via Z-brain in wild-type and *dscaml1*^{-/-} fish. **(A,B)** Heat map of normalized signals in major anatomical regions from Z-brain showing normalized signals detected within each sample used for analysis, wild-type ($n = 24$) and *dscaml1*^{-/-} ($n = 26$), and their corresponding neuron types **(A)** is excitatory while **(B)** is inhibitory. All signals were descended aligning to Diencephalon.

Supplementary Video 1 | Image stack of TRAS-labeled zebrafish larva, 3 days after the initial infection. VSV Δ G labeling is shown in magenta and *vglut2a:GFP* labeling in green.

Supplementary Video 2 | Excitatory (green) and inhibitory (magenta) retinorecipient cells in wild type **(Left)** and *dscaml1*^{-/-} **(Right)** cohorts. ERK1/2 immunolabeling (white) from Randlett et al. (2015) is overlaid to serve as an anatomical reference.

REFERENCES

- Abdelfattah, A. S., Kawashima, T., Singh, A., Novak, O., Liu, H., Shuai, Y., et al. (2019). Bright and photostable chemigenetic indicators for extended *in vivo* voltage imaging. *Science* 365, 699–704. doi: 10.1126/science.aav6416
- Ahmed, M., and Lyles, D. S. (1998). Effect of vesicular stomatitis virus matrix protein on transcription directed by host RNA polymerases I, II, and III. *J. Virol.* 72, 8413–8419. doi: 10.1128/JVI.72.10.8413-8419.1998
- Ahrens, M. B., Orger, M. B., Robson, D. N., Li, J. M., and Keller, P. J. (2013). Whole-brain functional imaging at cellular resolution using light-sheet microscopy. *Nat. Methods* 10, 413–420. doi: 10.1038/nmeth.2434
- Albertini, A. A., Baquero, E., Ferlin, A., and Gaudin, Y. (2012). Molecular and cellular aspects of rhabdovirus entry. *Viruses* 4, 117–139. doi: 10.3390/v4010117
- Amirache, F., Lévy, C., Costa, C., Mangeot, P.-E., Torbett, B. E., Wang, C. X., et al. (2014). Mystery solved: VSV-G-LVs do not allow efficient gene transfer into unstimulated T cells, B cells, and HSCs because they lack the LDL receptor. *Blood* 123:1422. doi: 10.1182/blood-2013-11-540641
- Amo, R., Aizawa, H., Takahoko, M., Kobayashi, M., Takahashi, R., Aoki, T., et al. (2010). Identification of the zebrafish ventral habenula as a homolog of the mammalian lateral habenula. *J. Neurosci.* 30, 1566–1574. doi: 10.1523/JNEUROSCI.3690-09.2010
- Ang, A. L., Taguchi, T., Francis, S., Folsch, H., Murrells, L. J., Pypaert, M., et al. (2004). Recycling endosomes can serve as intermediates during transport from the Golgi to the plasma membrane of MDCK cells. *J. Cell Biol.* 167, 531–543. doi: 10.1083/jcb.200408165
- Bae, Y. K., Kani, S., Shimizu, T., Tanabe, K., Nojima, H., Kimura, Y., et al. (2009). Anatomy of zebrafish cerebellum and screen for mutations affecting its development. *Dev. Biol.* 330, 406–426. doi: 10.1016/j.ydbio.2009.04.013
- Beier, K. T. (2019). Hitchhiking on the neuronal highway: mechanisms of transsynaptic specificity. *J. Chem. Neuroanat.* 99, 9–17. doi: 10.1016/j.jchemneu.2019.05.001
- Beier, K. T., Mundell, N. A., Pan, Y. A., and Cepko, C. L. (2016). Anterograde or retrograde transsynaptic circuit tracing in vertebrates with vesicular stomatitis virus vectors. *Curr. Protoc. Neurosci.* 74, 1.26.21–1.26.27. doi: 10.1002/0471142301.ns0126s74
- Beier, K. T., Samson, M. E. S., Matsuda, T., and Cepko, C. L. (2011a). Conditional expression of the TVA receptor allows clonal analysis of descendants from Cre-expressing progenitor cells. *Dev. Biol.* 353, 309–320. doi: 10.1016/j.ydbio.2011.03.004

- Beier, K. T., Saunders, A., Oldenburg, I. A., Miyamichi, K., Akhtar, N., Luo, L., et al. (2011b). Anterograde or retrograde transsynaptic labeling of CNS neurons with vesicular stomatitis virus vectors. *Proc. Natl. Acad. Sci. U.S.A.* 108, 15414–15419. doi: 10.1073/pnas.1110854108
- Beier, K. T., Saunders, A. B., Oldenburg, I. A., Sabatini, B. L., and Cepko, C. L. (2013). Vesicular stomatitis virus with the rabies virus glycoprotein directs retrograde transsynaptic transport among neurons *in vivo*. *Front. Neural Circuits* 7:11. doi: 10.3389/fncir.2013.00011
- Belmonte, M. K., Allen, G., Beckel-Mitchener, A., Boulanger, L. M., Carper, R. A., and Webb, S. J. (2004). Autism and abnormal development of brain connectivity. *J. Neurosci.* 24, 9228–9231. doi: 10.1523/JNEUROSCI.3340-04.2004
- Bianco, I. H., and Wilson, S. W. (2009). The habenular nuclei: a conserved asymmetric relay station in the vertebrate brain. *Philos. Trans. R. Soc. London Ser. B Biol. Sci.* 364, 1005–1020. doi: 10.1098/rstb.2008.0213
- Burrill, J. D., and Easter, S. S. Jr. (1994). Development of the retinofugal projections in the embryonic and larval zebrafish (*Brachydanio rerio*). *J. Comp. Neurol.* 346, 583–600. doi: 10.1002/cne.903460410
- Callaway, E. M., and Luo, L. (2015). Monosynaptic circuit tracing with glycoprotein-deleted rabies viruses. *J. Neurosci.* 35:8979. doi: 10.1523/JNEUROSCI.0409-15.2015
- Chatterjee, S., Sullivan, H. A., MacLennan, B. J., Xu, R., Hou, Y., Lavin, T. K., et al. (2018). Nontoxic, double-deletion-mutant rabies viral vectors for retrograde targeting of projection neurons. *Nat. Neurosci.* 21, 638–646. doi: 10.1038/s41593-018-0091-7
- Chen, X., Mu, Y., Hu, Y., Kuan, A. T., Nikitchenko, M., Randlett, O., et al. (2018). Brain-wide organization of neuronal activity and convergent sensorimotor transformations in larval zebrafish. *Neuron* 100, 876–890.e875. doi: 10.1016/j.neuron.2018.09.042
- Chou, M.-Y., Amo, R., Kinoshita, M., Cherng, B.-W., Shimazaki, H., Agetsuma, M., et al. (2016). Social conflict resolution regulated by two dorsal habenular subregions in zebrafish. *Science* 352, 87–90. doi: 10.1126/science.aac9508
- Ciabatti, E., Gonzalez-Rueda, A., Mariotti, L., Morgese, F., and Tripodi, M. (2017). Life-long genetic and functional access to neural circuits using self-inactivating rabies virus. *Cell* 170, 382–392.e314. doi: 10.1016/j.cell.2017.06.014
- Connor, J. H., and Lyles, D. S. (2005). Inhibition of host and viral translation during vesicular stomatitis virus infection. eIF2 is responsible for the inhibition of viral but not host translation. *J. Biol. Chem.* 280, 13512–13519. doi: 10.1074/jbc.M501156200
- Cui, W. W., Low, S. E., Hirata, H., Saint-Amant, L., Geisler, R., Hume, R. I., et al. (2005). The Zebrafish *shocked* gene encodes a glycine transporter and is essential for the function of early neural circuits in the CNS. *J. Neurosci.* 25, 6610–6620. doi: 10.1523/JNEUROSCI.5009-04.2005
- Deciphering Developmental Disorders Study (2017). Prevalence and architecture of *de novo* mutations in developmental disorders. *Nature* 542, 433–438. doi: 10.1038/nature21062
- Dohaku, R., Yamaguchi, M., Yamamoto, N., Shimizu, T., Osakada, F., and Hibi, M. (2019). Tracing of afferent connections in the zebrafish cerebellum using recombinant rabies virus. *Front. Neural Circuits* 13:30. doi: 10.3389/fncir.2019.00030
- Dotti, C. G., and Simons, K. (1990). Polarized sorting of viral glycoproteins to the axon and dendrites of hippocampal neurons in culture. *Cell* 62, 63–72. doi: 10.1016/0092-8674(90)90240-F
- Dreosti, E., Vendrell Llopis, N., Carl, M., Yaksi, E., and Wilson, S. W. (2014). Left-right asymmetry is required for the habenulae to respond to both visual and olfactory stimuli. *Curr. Biol.* 24, 440–445. doi: 10.1016/j.cub.2014.01.016
- Duboue, E. R., Hong, E., Eldred, K. C., and Halpern, M. E. (2017). Left habenular activity attenuates fear responses in larval zebrafish. *Curr. Biol.* 27, 2154–2162.e2153. doi: 10.1016/j.cub.2017.06.017
- Feng, L., Zhao, T., and Kim, J. (2015). neuTube 1.0: a new design for efficient neuron reconstruction software based on the SWC format. *eNeuro* 2:ENEURO.0049-14.2014. doi: 10.1523/ENEURO.0049-14.2014
- Finkelshtein, D., Werman, A., Novick, D., Barak, S., and Rubinstein, M. (2013). LDL receptor and its family members serve as the cellular receptors for vesicular stomatitis virus. *Proc. Natl. Acad. Sci. U.S.A.* 110, 7306–7311. doi: 10.1073/pnas.1214441110
- Fornito, A., Zalesky, A., and Breakspear, M. (2015). The connectomics of brain disorders. *Nat. Rev. Neurosci.* 16:159. doi: 10.1038/nrn3901
- Fossati, M., Colombo, S. F., and Borgese, N. (2014). A positive signal prevents secretory membrane cargo from recycling between the Golgi and the ER. *EMBO J.* 33, 2080–2097. doi: 10.15252/embj.201488367
- Fuerst, P. G., Bruce, F., Tian, M., Wei, W., Elstrott, J., Feller, M. B., et al. (2009). DSCAM and DSCAML1 function in self-avoidance in multiple cell types in the developing mouse retina. *Neuron* 64, 484–497. doi: 10.1016/j.neuron.2009.09.027
- Galicía, C. A., Sukeena, J. M., Stenkamp, D. L., and Fuerst, P. G. (2018). Expression patterns of *dscam* and *sdk* gene paralogs in developing zebrafish retina. *Mol. Vis.* 24, 443–458.
- Glasser, M. F., Coalson, T. S., Robinson, E. C., Hacker, C. D., Harwell, J., Yacoub, E., et al. (2016). A multi-modal parcellation of human cerebral cortex. *Nature* 536:171. doi: 10.1038/nature18933
- Helmbrecht, T. O., Dal Maschio, M., Donovan, J. C., Koutsouli, S., and Baier, H. (2018). Topography of a visuomotor transformation. *Neuron* 100, 1429–1445.e4. doi: 10.1016/j.neuron.2018.10.021
- Hildebrand, D. G. C., Cicconet, M., Torres, R. M., Choi, W., Quan, T. M., Moon, J., et al. (2017). Whole-brain serial-section electron microscopy in larval zebrafish. *Nature* 545, 345–349. doi: 10.1038/nature22356
- Hoffmann, M., Wu, Y. J., Gerber, M., Berger-Rentsch, M., Heimrich, B., Schwemmler, M., et al. (2010). Fusion-active glycoprotein G mediates the cytotoxicity of vesicular stomatitis virus M mutants lacking host shut-off activity. *J. Gen. Virol.* 91, 2782–2793. doi: 10.1099/vir.0.023978-0
- Iossifov, I., O’Roak, B. J., Sanders, S. J., Ronemus, M., Krumm, N., Levy, D., et al. (2014). The contribution of *de novo* coding mutations to autism spectrum disorder. *Nature* 515, 216–221. doi: 10.1038/nature13908
- Jefferis, G. S., Potter, C. J., Chan, A. M., Marin, E. C., Rohlffing, T., Maurer, C. R. Jr., et al. (2007). Comprehensive maps of *Drosophila* higher olfactory centers: spatially segregated fruit and pheromone representation. *Cell* 128, 1187–1203. doi: 10.1016/j.cell.2007.01.040
- Karaca, E., Harel, T., Pehlivan, D., Jhangiani, S. N., Gambin, T., Coban Akdemir, Z., et al. (2015). Genes that affect brain structure and function identified by rare variant analyses of mendelian neurologic disease. *Neuron* 88, 499–513. doi: 10.1016/j.neuron.2015.09.048
- Kasthuri, N., Hayworth, K. J., Berger, D. R., Schalek, R. L., Conchello, J. A., Knowles-Barley, S., et al. (2015). Saturated reconstruction of a volume of neocortex. *Cell* 162, 648–661. doi: 10.1016/j.cell.2015.06.054
- Kawashima, T., Zwart, M. F., Yang, C. T., Mensh, B. D., and Ahrens, M. B. (2016). The serotonergic system tracks the outcomes of actions to mediate short-term motor learning. *Cell* 167, 933–946.e920. doi: 10.1016/j.cell.2016.09.055
- Kim, I. S., Jenni, S., Stanifer, M. L., Roth, E., Whelan, S. P., van Oijen, A. M., et al. (2017). Mechanism of membrane fusion induced by vesicular stomatitis virus G protein. *Proc. Natl. Acad. Sci. U.S.A.* 114, E28–E36. doi: 10.1073/pnas.1618883114
- Kimmel, C. B., Ballard, W. W., Kimmel, S. R., Ullmann, B., and Schilling, T. F. (1995). Stages of embryonic development of the zebrafish. *Dev. Dyn.* 203, 253–310. doi: 10.1002/aja.1002030302
- Kobayashi, K., Kato, S., Inoue, K., Takada, M., and Kobayashi, K. (2016). Altering entry site preference of lentiviral vectors into neuronal cells by pseudotyping with envelope glycoproteins. *Methods Mol. Biol.* 1382, 175–186. doi: 10.1007/978-1-4939-3271-9_12
- Kramer, A., Wu, Y., Baier, H., and Kubo, F. (2019). Neuronal architecture of a visual center that processes optic flow. *Neuron* 103, 118–132.e7. doi: 10.1016/j.neuron.2019.04.018
- Kunst, M., Laurell, E., Mokayes, N., Kramer, A., Kubo, F., Fernandes, A. M., et al. (2019). A cellular-resolution atlas of the larval zebrafish brain. *Neuron* 103, 21–38.e5. doi: 10.2139/ssrn.3257346
- Lee, A., Mathuru, A. S., Teh, C., Kibat, C., Korzh, V., Penney, T. B., et al. (2010). The habenula prevents helpless behavior in larval zebrafish. *Curr. Biol.* 20, 2211–2216. doi: 10.1016/j.cub.2010.11.025
- Li, L., and Dowling, J. E. (2000). Disruption of the olfactoryretinal centrifugal pathway may relate to the visual system defect in night blindness b mutant zebrafish. *J. Neurosci.* 20, 1883–1892. doi: 10.1523/JNEUROSCI.20-05-01883.2000
- Lynall, M.-E., Bassett, D. S., Kerwin, R., McKenna, P. J., Kitzbichler, M., Muller, U., et al. (2010). Functional connectivity and brain networks in schizophrenia. *J. Neurosci.* 30, 9477–9487. doi: 10.1523/JNEUROSCI.0333-10.2010

- Ma, M., Ramirez, A. D., Wang, T., Roberts, R. L., Harmon, K. E., Schoppik, D., et al. (2020). Zebrafish *dscaml1* deficiency impairs retinal patterning and oculomotor function. *J. Neurosci.* 40, 143–158. doi: 10.1523/JNEUROSCI.1783-19.2019
- Maack, G., and Segner, H. (2003). Morphological development of the gonads in zebrafish. *J. Fish Biol.* 62, 895–906. doi: 10.1046/j.1095-8649.2003.00074.x
- Miyamichi, K., Amat, F., Moussavi, F., Wang, C., Wickersham, I., Wall, N. R., et al. (2011). Cortical representations of olfactory input by trans-synaptic tracing. *Nature* 472, 191–196. doi: 10.1038/nature09714
- Mueller, T. (2012). What is the thalamus in zebrafish? *Front. Neurosci.* 6, 64–64. doi: 10.3389/fnins.2012.00064
- Mueller, T., Vernier, P., and Wullimann, M. F. (2006). A phylotypic stage in vertebrate brain development: GABA cell patterns in zebrafish compared with mouse. *J. Comp. Neurol.* 494, 620–634. doi: 10.1002/cne.20824
- Mueller, T. W., and Wullimann, M. F. (2015). *Atlas of Early Zebrafish Brain Development: A Tool for Molecular Neurogenetics*. Boston, MA: Elsevier.
- Mundell, N. A., Beier, K. T., Pan, Y. A., Lapan, S. W., Goz Ayturk, D., Berezovskii, V. K., et al. (2015). Vesicular stomatitis virus enables gene transfer and transsynaptic tracing in a wide range of organisms. *J. Comp. Neurol.* 523, 1639–1663. doi: 10.1002/cne.23761
- Muto, A., Ohkura, M., Abe, G., Nakai, J., and Kawakami, K. (2013). Real-time visualization of neuronal activity during perception. *Curr. Biol.* 23, 307–311. doi: 10.1016/j.cub.2012.12.040
- Oh, S. W., Harris, J. A., Ng, L., Winslow, B., Cain, N., Mihalas, S., et al. (2014). A mesoscale connectome of the mouse brain. *Nature* 508, 207–214. doi: 10.1038/nature13186
- Orger, M. B., and de Polavieja, G. G. (2017). Zebrafish behavior: opportunities and challenges. *Annu. Rev. Neurosci.* 40, 125–147. doi: 10.1146/annurev-neuro-071714-033857
- Randlett, O., Wee, C. L., Naumann, E. A., Nnaemeka, O., Schoppik, D., Fitzgerald, J. E., et al. (2015). Whole-brain activity mapping onto a zebrafish brain atlas. *Nat. Methods* 12, 1039–1046. doi: 10.1038/nmeth.3581
- Robles, E., Laurell, E., and Baier, H. (2014). The retinal projectome reveals brain-area-specific visual representations generated by ganglion cell diversity. *Curr. Biol.* 24, 2085–2096. doi: 10.1016/j.cub.2014.07.080
- Rohlfing, T., and Maurer, C. R. (2003). Nonrigid image registration in shared-memory multiprocessor environments with application to brains, breasts, and bees. *IEEE Trans. Inform. Technol. Biomed.* 7, 16–25. doi: 10.1109/TITB.2003.808506
- Sakai, C., Ijaz, S., and Hoffman, E. J. (2018). Zebrafish models of neurodevelopmental disorders: past, present, and future. *Front. Mol. Neurosci.* 11:294. doi: 10.3389/fnmol.2018.00294
- Sato, T., Hamaoka, T., Aizawa, H., Hosoya, T., and Okamoto, H. (2007). Genetic single-cell mosaic analysis implicates ephrinB2 reverse signaling in projections from the posterior tectum to the hindbrain in zebrafish. *J. Neurosci.* 27, 5271–5279. doi: 10.1523/JNEUROSCI.0883-07.2007
- Satou, C., Kimura, Y., Hirata, H., Suster, M. L., Kawakami, K., and Higashijima, S. (2013). Transgenic tools to characterize neuronal properties of discrete populations of zebrafish neurons. *Development* 140, 3927–3931. doi: 10.1242/dev.099531
- Spickler, A. R. (2016). *Vesicular Stomatitis*. Available online at: <http://www.cfsph.iastate.edu/DiseaseInfo/factsheets.php> (accessed July 16, 2019).
- Stuermer, C. A. (1988). Retinotopic organization of the developing retinotectal projection in the zebrafish embryo. *J. Neurosci.* 8, 4513–4530. doi: 10.1523/JNEUROSCI.08-12-04513.1988
- Svara, F. N., Kornfeld, J., Denk, W., and Bollmann, J. H. (2018). Volume EM reconstruction of spinal cord reveals wiring specificity in speed-related motor circuits. *Cell Rep.* 23, 2942–2954. doi: 10.1016/j.celrep.2018.05.023
- Swanson, L. W., and Lichtman, J. W. (2016). From cajal to connectome and beyond. *Annu. Rev. Neurosci.* 39, 197–216. doi: 10.1146/annurev-neuro-071714-033954
- Thomas, D. C., Brewer, C. B., and Roth, M. G. (1993). Vesicular stomatitis virus glycoprotein contains a dominant cytoplasmic basolateral sorting signal critically dependent upon a tyrosine. *J. Biol. Chem.* 268, 3313–3320.
- Thyme, S. B., Pieper, L. M., Li, E. H., Pandey, S., Wang, Y., Morris, N. S., et al. (2019). Phenotypic landscape of schizophrenia-associated genes defines candidates and their shared functions. *Cell* 177, 478–491.e420. doi: 10.1016/j.cell.2019.01.048
- Vishwanathan, A., Daie, K., Ramirez, A. D., Lichtman, J. W., Aksay, E. R. F., and Seung, H. S. (2017). Electron microscopic reconstruction of functionally identified cells in a neural integrator. *Curr. Biol.* 27, 2137–2147.e2133. doi: 10.1016/j.cub.2017.06.028
- Wanner, A. A., Genoud, C., Masudi, T., Siksou, L., and Friedrich, R. W. (2016). Dense EM-based reconstruction of the interglomerular projectome in the zebrafish olfactory bulb. *Nat. Neurosci.* 19, 816–825. doi: 10.1038/nn.4290
- Watabe-Uchida, M., Zhu, L., Ogawa Sachie, K., Vamanrao, A., and Uchida, N. (2012). Whole-brain mapping of direct inputs to midbrain dopamine neurons. *Neuron* 74, 858–873. doi: 10.1016/j.neuron.2012.03.017
- Wickersham, I. R., Lyon, D. C., Barnard, R. J., Mori, T., Finke, S., Conzelmann, K. K., et al. (2007). Monosynaptic restriction of transsynaptic tracing from single, genetically targeted neurons. *Neuron* 53, 639–647. doi: 10.1016/j.neuron.2007.01.033
- Wickersham, I. R., Sullivan, H. A., and Seung, H. S. (2013). Axonal and subcellular labelling using modified rabies viral vectors. *Nat. Commun.* 4:2332. doi: 10.1038/ncomms3332
- Wilson, C. A., High, S. K., McCluskey, B. M., Amores, A., Yan, Y.-I., Titus, T. A., et al. (2014). Wild sex in zebrafish: loss of the natural sex determinant in domesticated strains. *Genetics* 198, 1291–1308. doi: 10.1534/genetics.114.169284
- Yang, B., Treweek, J. B., Kulkarni, R. P., Deverman, B. E., Chen, C. K., Lubeck, E., et al. (2014). Single-cell phenotyping within transparent intact tissue through whole-body clearing. *Cell* 158, 945–958. doi: 10.1016/j.cell.2014.07.017
- Yee, J. K., Miyanohara, A., LaPorte, P., Bouic, K., Burns, J. C., and Friedmann, T. (1994). A general method for the generation of high-titer, pantropic retroviral vectors: highly efficient infection of primary hepatocytes. *Proc. Natl. Acad. Sci. U.S.A.* 91, 9564–9568. doi: 10.1073/pnas.91.20.9564
- Zhang, B. B., Yao, Y. Y., Zhang, H. F., Kawakami, K., and Du, J. L. (2017). Left habenula mediates light-preference behavior in zebrafish via an asymmetrical visual pathway. *Neuron* 93, 914–928.e914. doi: 10.1016/j.neuron.2017.01.011
- Zhu, P., Narita, Y., Bundschuh, S. T., Fajardo, O., Scharer, Y. P., Chattopadhyaya, B., et al. (2009). Optogenetic dissection of neuronal circuits in zebrafish using viral gene transfer and the tet system. *Front. Neural Circuits* 3:21. doi: 10.3389/neuro.04.021.2009
- Zingg, B., Chou, X. L., Zhang, Z. G., Mesik, L., Liang, F., Tao, H. W., et al. (2017). AAV-mediated anterograde transsynaptic tagging: mapping corticocollicular input-defined neural pathways for defense behaviors. *Neuron* 93, 33–47. doi: 10.1016/j.neuron.2016.11.045

Conflict of Interest: The authors declare that the research was conducted in the absence of any commercial or financial relationships that could be construed as a potential conflict of interest.

Copyright © 2020 Ma, Kler and Pan. This is an open-access article distributed under the terms of the Creative Commons Attribution License (CC BY). The use, distribution or reproduction in other forums is permitted, provided the original author(s) and the copyright owner(s) are credited and that the original publication in this journal is cited, in accordance with accepted academic practice. No use, distribution or reproduction is permitted which does not comply with these terms.